

Rock-physics templates for clay-rich source rocks

José M. Carcione¹ and Per Avseth²

ABSTRACT

Shale source rocks are composed of various minerals, mainly smectite and illite, depending on the burial depth, and they can be described as transversely isotropic media. The “pore space” may contain kerogen, water, oil, and gas determined by the in situ conditions. A petroelastic description is based on the following: Smectite-illite transformation as a function of depth is described by a fifth-order kinetic reaction. Backus averaging to “mix” isotropic smectite and anisotropic illite is then used to obtain the elasticity constants of the mineral composing the frame. Porosity is obtained from density, and water is part of the mineral, whose elasticity constants are obtained from Gassmann equations. Oil and gas generated from kerogen are assumed to saturate the kerogen phase. The bulk modulus of the oil-gas mixture is calculated by a mesoscopic-loss model, and the stiffnesses of the kerogen/fluid mixture are obtained with the Kuster and Toksöz model, assuming that the fluid is included in

a kerogen matrix. Two models are considered to obtain the seismic velocities of the shale, namely, Backus averaging and the Gassmann equation generalized to the anisotropic case with a solid pore infill. We built rock-physics templates (RPTs) containing only kerogen (immature) and kerogen plus hydrocarbons (mature). Pore-pressure effects were modeled and used as templates. We considered the Kimmeridge Shale at different depths. To model kerogen-oil and oil-gas conversions, we assumed a basin-evolution model with a constant sedimentation rate, geothermal gradient, and a first-order kinetic (Arrhenius) reaction. The detection of the hydrocarbons was investigated from RPTs, built with wave velocities, impedances, Lamé constants, density, Poisson ratio, Young modulus, and anisotropy parameters for varying kerogen content, fluid saturations, and pore pressure. Moreover, the amplitude variation with offset intercept and gradients were computed, corresponding to the seismic response of a source rock layer for varying kerogen content and fluid saturation.

INTRODUCTION

Rock-physics templates (RPTs) establish a link between the elastic properties (e.g., velocity, density, impedance, and wet-rock stiffness moduli) and the reservoir properties, such as porosity, fluid saturation and clay content in sandstones or kerogen content, and hydrocarbon saturation in source rocks. Specific examples can be found in Ødegaard and Avseth (2004), Avseth et al. (2005), and Chi and Han (2009). Building a template requires calibration with well-log data. There are several steps to calibrate and use the templates: (1) obtain the effective properties of the grain minerals and pore-infill material, (2) determine the properties of the dry rock, (3) obtain the wet-rock velocities and mass density with a suitable model (Backus averaging and the Gassmann equation are used here), (4) perform pore-infill substitution to determine the location of each

specific pore-infill component in the RPT, and (5) report the seismic properties on the templates to create total organic content (TOC) and fluid saturation maps of the studied area.

In the case of source rocks, the analysis with RPT is scarce. Zhu et al. (2012, 2013) use the Gassmann-type model developed by Carcione et al. (2011) to incorporate TOC effects, mineralogy, porosity, and fluid content, and they describe the seismic properties of source rocks. Their modeling indicates that an increase in TOC generally reduces the P-wave impedance and the V_P/V_S ratio, increasing the velocity anisotropy, as already shown by Carcione (2000), where V_P and V_S denote the P- and S-wave velocities. Cerón et al. (2013) analyze several shale cores of the Cretaceous Colombian basin showing the presence of organic content. Density crossplots and permeability-porosity templates are shown. Yenugu and Han (2013) use Carcione's (2000) approach to model the degree of

Manuscript received by the Editor 4 November 2014; revised manuscript received 9 February 2015; published online 17 July 2015.

¹Istituto Nazionale di Oceanografia e di Geofisica Sperimentale, Trieste, Italy. E-mail: jcarcione@inogs.it.

²Norwegian University of Science and Technology, Oslo, Trondheim, Norway and Tullow Oil, Oslo, Trondheim, Norway. E-mail: per.avseth@tullowoil.com.

© 2015 Society of Exploration Geophysicists. All rights reserved.

maturity of the shale and obtain its elastic properties and related amplitude variation with offset (AVO) effects. Bakken shale has class IV AVO, and its amplitude is affected by kerogen maturity.

Oil and gas can be generated in kerogen-rich shales at the oil and gas windows, where the amount of conversion depends on temperature. Carcione (2000) and Pinna et al. (2011) quantify the conversion as a function of the sedimentation rate and geothermal gradient using the Arrhenius equation. The model assumes one reaction rate and a closed system; here, we assume that the kerogen-to-gas conversion is negligible (gas is generated from oil). As Pepper and Corvi (1995) state: “gas yields directly from kerogen are not the prime causes of gas proneness in source rocks.” On the other hand, the conversion from smectite to illite (clay diagenesis) with increasing depth occurs in all shales (Scotchman, 1987) and can be described by the widely accepted model proposed by Pytte and Reynolds (1989) based on a fifth-order kinetic reaction of the Arrhenius type. The result of the conversion is that the stiffnesses of the mineral composing the shale increase with depth. Backus averaging is then used to obtain the properties of the smectite-illite mixture.

Research conducted by Vernik and Nur (1992), Vernik (1994, 1995), and Vernik and Landis (1996) on petroleum source rocks indicates that strong velocity anisotropy is associated with the presence of organic matter and the layered nature of the single components. Vernik (1995) and Carcione (2000) use Backus averaging to describe the elastic properties. Carcione et al. (2011) use Ciz and Shapiro's (2007) (Gassmann) equation for an anisotropic frame and an isotropic solid pore infill (kerogen-oil) (Ba et al., 2015). The dry-rock elasticity constants involved in the Gassmann equation are obtained by a generalization of Krief equations to the anisotropic case (see the isotropic version in Krief et al., 1990). In this case, by “dry rock,” we mean the rock excluding the pore-fill (kerogen, water, oil, and gas), whereas “wet rock” refers to the rock including the pore-fill. Bound water is part of the rock frame. Figure 1 shows a scheme in which porosity is defined according to the elastic model used. The effect of partial saturation on velocity depends on the location of the so-called mesoscopic-loss peak in the frequency axis (e.g.,

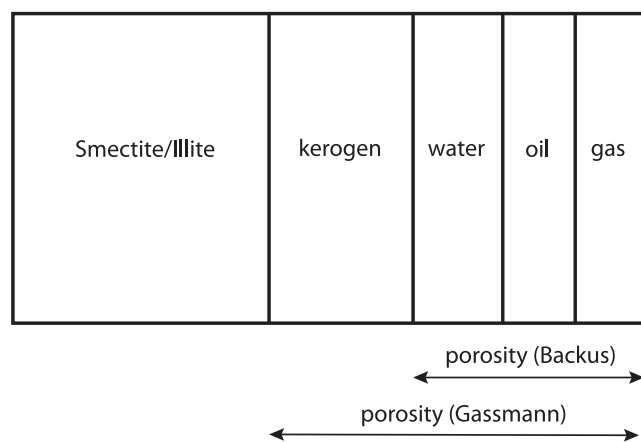


Figure 1. Organic shale components indicating the “porosity” corresponding to the Backus and Gassmann models. The porosity in the case of the Gassmann model includes the solid pore infill. The actual porosity ϕ of the rock to calculate the fluid saturations is that indicated for the Backus model, i.e., the sum of the water, oil, and gas proportions. The organic content porosity ϕ_{OC} is the sum of the kerogen, oil, and gas proportions.

Carcione and Picotti, 2006; Carcione, 2015). When oil and gas are generated in a kerogen matrix, the gas bubbles embedded in the oil cause a wave-induced fluid-flow attenuation mechanism, which yields velocity dispersion. The location of the peak depends mainly on the size of the gas pockets, and the bulk modulus of the fluid mixture differs from the Wood (or Reuss) modulus. The model used to compute the modulus is based on White theory (e.g., Carcione, 2015). On the other hand, the PP reflection coefficients of a source-rock layer as a function of the layer thickness and organic content has been obtained by Carcione (2001b). Here, we analyze the AVO class of a thin source-rock layer from AVO crossplotting based on Shuey's two-term approximation. Details of the algorithms to compute the scattering coefficients can be found in Carcione (2001a, 2001b).

KEROGEN/OIL/GAS AND SMECTITE/ILLITE CONVERSIONS

To obtain the fraction of oil and gas at a given depth, we assume: (1) no loss of fluid from the source-rock pore volume (a closed system with negligible permeability); (2) the initial pore volume contains only convertible kerogen because the water content is relatively small and is part of the matrix (smectite/illite); and (3) kerogen/oil and oil/gas conversion are two independent processes (Berg and Gangi, 1999). The model is given in Appendix A and considers two separate kinetic reactions describing the kerogen/oil and oil/gas conversions.

Moreover, it is important to evaluate the amount of the smectite/illite ratio forming the shale matrix because this ratio affects the stiffness moduli and wave velocities of the rock. Shale mineralogy may include kaolinite, montmorillonite-smectite, illite, and chlorite, so the term *smectite-illite* as used in this study may be representative for a mixture of clay minerals (Mondol et al., 2008). In the Kimmeridge Clay, there is also some percentage of silty quartz (Williams et al., 2001). Moreover, the smectite-illite layers represent an assembly of platelets, subject to internal hydration, so its mechanical properties such as the stiffnesses can vary depending on the source rock.

The conversion smectite/illite occurs in all shales with a general release of bound water into the pore space (Scotchman, 1987). Smectite dehydration implies a stiffer matrix due to the presence of more illite and therefore higher velocities. The conversion depends on the temperature and sedimentation rate. A solution to this problem has been provided by Pytte and Reynolds (1989) (see Appendix A). Smectite and illite are then “mixed” by Backus averaging (e.g., Carcione, 2015) to obtain the elasticity constants of the mineral composing the frame.

The example shown here corresponds to a clay-rich source rock (Kimmeridge Clay). However, there are other source rocks that are rich in quartz or calcite. To include these minerals, the properties of the composite rock frame can be obtained as the arithmetic average of the upper and lower Hashin-Shtrikman bounds (e.g., Carcione et al., 2005, 2006). The grain density is the arithmetic average of the densities of the single constituents weighted by the corresponding volume fractions.

Future works should consider another effect that could be important, i.e., quartz generation as a by-product of the diagenesis smectite/illite conversion. Thyberg et al. (2009) show that this is another factor to explain the velocity increase, due to microcrystalline quartz-cementation of the rock frame.

EFFECTIVE-MEDIA MODELS

We consider two models to obtain the stiffness moduli and wave velocities of the source rock, namely Backus averaging (Schoenberg and Muir, 1989; Vernik, 1994; Carcione, 2000; Carcione et al., 2011; Pinna et al., 2011) and the Gassmann equation for a solid pore infill (Ciz and Shapiro, 2007; Carcione et al., 2011; Ba et al., 2015). The rock geometry corresponding to these models is shown schematically in Figure 2, where Figure 2a depicts the model used by Backus to represent a system of plane layers whose thicknesses are much smaller compared with the wavelength of the signal, Figure 2b shows a modification of Backus model taking into account the discontinuity of the illite layers in the shale fabric, and Figure 2c is a representation of the shale based on Gassmann's assumptions to represent a porous medium. Regarding the model shown in Figure 2b, SEM observations have shown that the illite fabric has a lenticular pattern along the bedding plane rather than a continuous-layer structure (Vernik and Nur, 1992; Sayers, 2013). A reasonable way to model this effect is to substitute the bedding-plane elastic stiffnesses by a weighted average that takes into account the local proportion of illite and kerogen. In the Gassmann model, the pore space is continuous and can have any shape, as shown in Figure 2c (black area), and the liquid phase (hydrocarbons) generated by kerogen conversion is confined to that pore space.

We obtain the fluid properties as indicated in Carcione et al. (2006). In situ reservoir gas behaves as a real gas, which approximately satisfies the van der Waals equation. The liquid properties depend on temperature and pressure, as well as on the American Petroleum Institute (API) number and salinity, if the fluid is oil or water, respectively. Batzle and Wang (1992) and Mavko et al. (2009) provide a series of useful empirical relations between the state variables and velocity and density.

The mixture oil-gas behaves as a composite fluid with properties depending on the constants of the constituents and their relative concentrations. The simplest solution to obtain its bulk modulus is to assume the Wood average (see Appendix B). When the fluids are not mixed in the pore volume, but distributed in patches, the effective bulk modulus of the composite fluid is higher than that predicted by Wood equation. We assume a simplified model, based on White's (1975) theory, where the frame is the kerogen, and the fluids are oil and gas. White (1975) assumes spherical patches much larger than the grains, but much smaller than the wavelength (see Appendix B).

The stiffnesses of the kerogen/fluid mixture are calculated by the model developed by Kuster and Toksöz (1974), which assumes that the kerogen-oil-gas mixture consists of oil-gas bubbles embedded in a kerogen matrix (see Carcione, 2000; Carcione et al., 2006, 2011; Pinna et al., 2011). Calculation of the Gassmann moduli requires to know the dry-rock elasticity constants. These are obtained by a simple generalization of the Krief et al. (1990) model (see Carcione et al., 2011; Pinna et al., 2011).

The notation used in this article is the following (see Appendix D for a list of symbols): The quantities K , μ , and ρ indicate the bulk modulus, shear modulus, and density, respectively, and the indices m , s , w , o , g , f , k , and if denote the dry matrix (frame or skeleton), solid grain (clay minerals), water (brine), oil, gas, fluid (oil-gas mixture), kerogen, and pore infill (oil-gas-kerogen mixture), respectively. Moreover, c_{IJ} denotes the two-index notation for stiffnesses (Helbig, 1994), and ϕ denotes porosity or proportion of a given material.

The quantities to build the templates are given in the following. The P- and S-wave impedances are

$$I_P = \rho V_P^2, \quad I_S = \rho V_S^2, \quad (1)$$

respectively, the Lamé constants are

$$\lambda = \rho(V_P^2 - 2V_S^2), \quad \mu = \rho V_S^2, \quad (2)$$

three dynamic Poisson's ratios, corresponding to different directions, are (Carcione and Cavallini, 2002)

$$\nu_1 = \frac{\bar{c}_{12}\bar{c}_{33} - \bar{c}_{13}^2}{\bar{c}_{11}\bar{c}_{33} - \bar{c}_{13}^2}, \quad \nu_2 = \frac{\bar{c}_{13}(\bar{c}_{11} - \bar{c}_{12})}{\bar{c}_{11}\bar{c}_{33} - \bar{c}_{13}^2}, \quad \nu_3 = \frac{\bar{c}_{13}}{\bar{c}_{11} + \bar{c}_{12}}, \quad (3)$$

the anisotropy parameters are (Thomsen, 1986)

$$\epsilon = \frac{\bar{c}_{11} - \bar{c}_{33}}{2\bar{c}_{33}}, \quad \gamma = \frac{\bar{c}_{66} - \bar{c}_{55}}{2\bar{c}_{55}}, \quad \delta = \frac{(\bar{c}_{13} + \bar{c}_{55})^2 - (\bar{c}_{33} - \bar{c}_{55})^2}{2\bar{c}_{33}(\bar{c}_{33} - \bar{c}_{55})}, \quad (4)$$

and the Young modulus is defined as

$$Y = 2\bar{c}_{55}(1 + \nu_i), \quad i = 1, 2, 3. \quad (5)$$

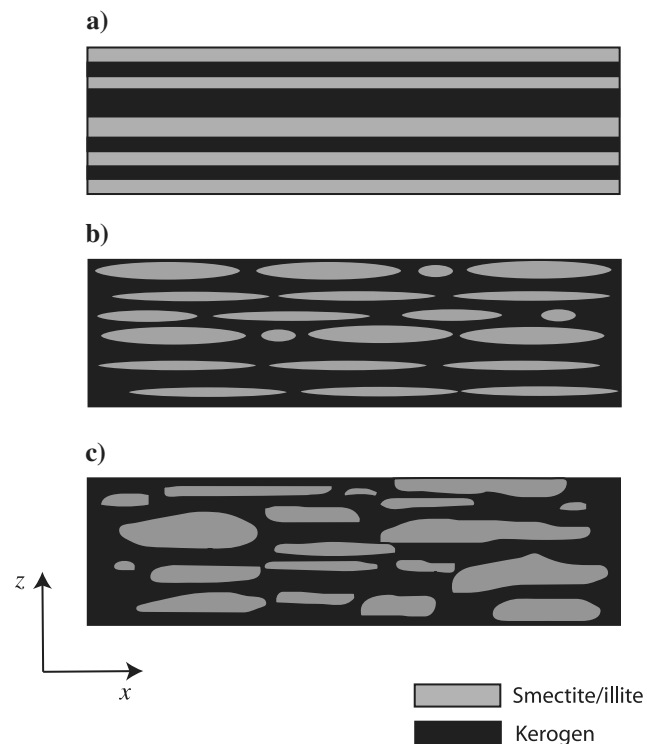


Figure 2. Schematic fabric topology of transversely isotropic kerogen-rich shales, according to the (a) Backus model, (b) modified Backus model and (c) Gassmann model. The z -direction corresponds to the symmetry axis.

See Carcione (2001a, 2001b) to obtain the AVO intercept and gradient and identify the AVO classes of a source-rock layer.

The modeling methodology and the different templates generated in this work are illustrated in Figure 3, where the various methods/equations are given. The main assumptions are that there is no loss of fluid from the source-rock pore volume when oil and gas are generated, water content is part of the matrix, and the kerogen/oil and oil/gas conversion are two independent processes. Moreover, effects due to seismic attenuation are neglected.

MODEL CALIBRATION

We consider the Spekk Formation (a Kimmeridge Shale equivalent in the Norwegian Sea). This formation is an Upper Jurassic to Lower Cretaceous black shale located on the mid-Norwegian shelf (Langrock, 2004). We have wireline logs from three wells, with

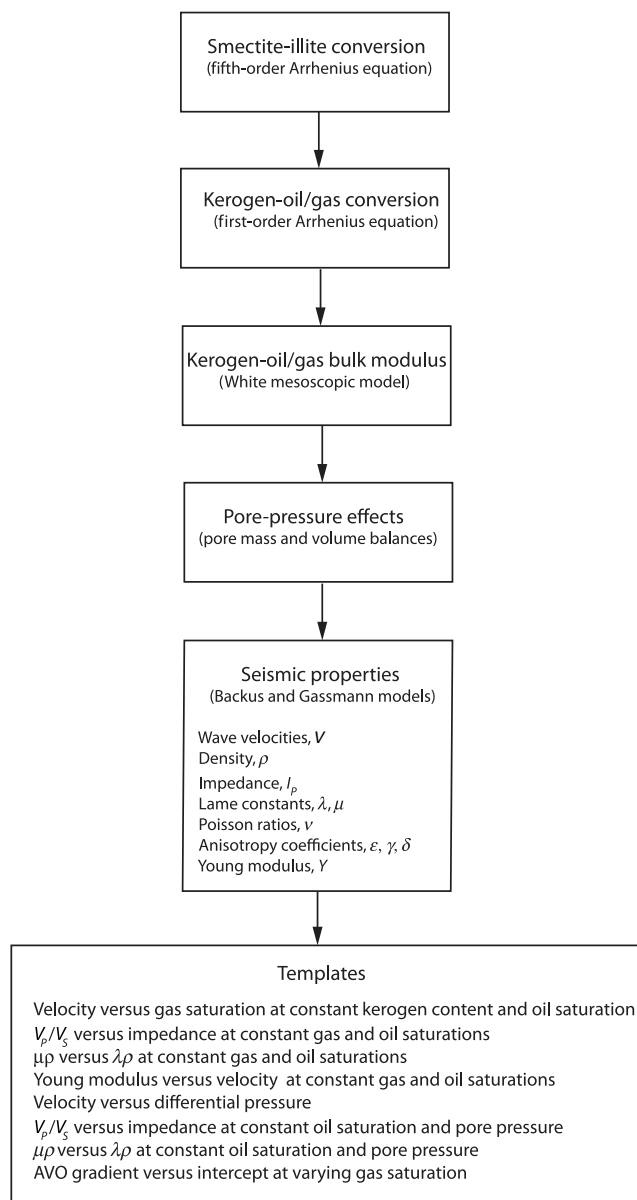


Figure 3. Modeling methodology and RPT.

average burial depths of 1.7, 2.4, and 2.6 km (wells 1, 2, and 3, respectively; water depths range between 300 and 500 m). Wells 1 and 3 are used for the calibration. First, we quantify the oil and gas saturations as a function of depth due to kerogen and oil conversions, respectively. As Berg and Gangi (1999), we consider a single activation energy. The “J70 Upper Jurassic Kimmeridge Clay Formation” is indicated as organofacies B in Pepper and Corvi (1995). The geothermal gradient in the studied area is $G = 37^\circ\text{C}/\text{km}$ (well reports), the sedimentation rate is $S = 0.04 \text{ mm}/\text{y}$ (Ebukanson and Kinghorn, 1990), and the surface temperature is 4°C . The assumed activation energies are $E = 28 \text{ kcal}/\text{mol}$ (kerogen/oil) and $E = 30 \text{ kcal}/\text{mol}$ (oil/gas), whereas the infinite-temperature rate is $A = 10^{13}/\text{m.y.}$ for oil and gas. Values of these parameters can be found in Pepper and Corvi (1995) and Berg and Gangi (1999) for instance. Figure 4a shows the fraction of kerogen converted to oil and the fraction of oil converted to gas. In principle, with these values of the kinetic parameters, the shale in well 1 has kerogen, whereas the shale in well 3 is partially saturated with oil. Assuming the properties of kerogen, oil, and water shown in Table 1 (at 3 km) and $S_w = 10\%$, Figure 4b displays the pore pressure generated due to the kerogen/oil conversion ($\phi' = 0.3$ in equation A-10

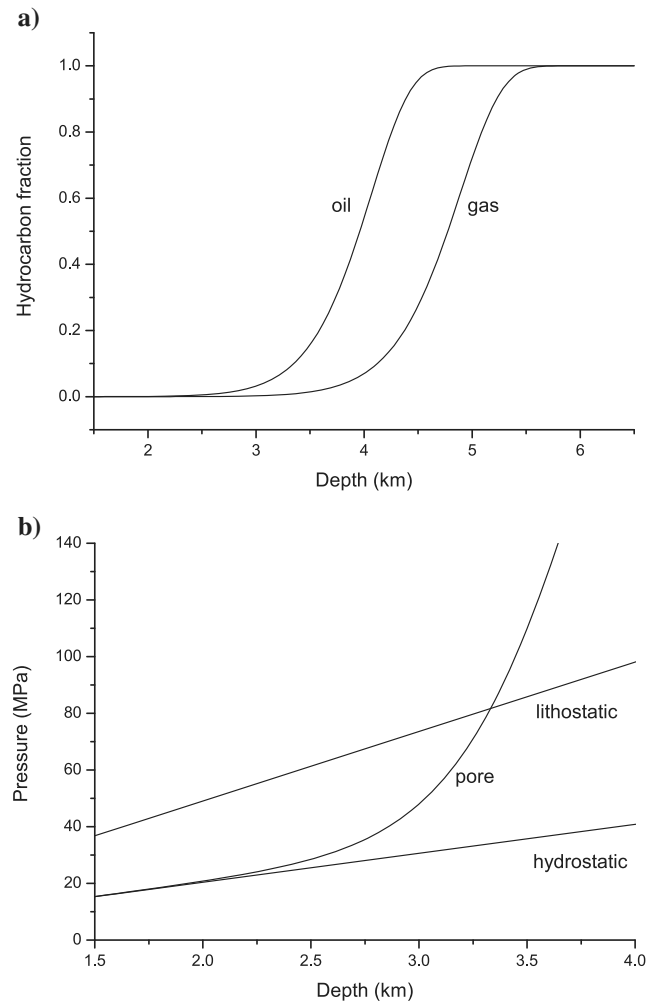


Figure 4. Kerogen/oil and oil/gas fractions as a function of (a) depth and (b) pore pressure generated due to the kerogen/oil conversion ($\phi' = 0.3$ in equation A-10 is assumed).

is assumed). The hydrostatic and lithostatic pressures are obtained as $p_H = \bar{\rho}_w g z$ and $p_c = \bar{\rho} g z$, respectively, where $\bar{\rho}_w = 1.04 \text{ g/cm}^3$, $\bar{\rho} = 2.4 \text{ g/cm}^3$, z is the depth, and $g = 9.81 \text{ m/s}^2$. Because oil cannot escape from the pore space (zero permeability), the pore pressure rapidly reaches the lithostatic pressure, where failure occurs. This happens at 3.3-km depth, where 10% of the kerogen has been converted to oil. However, this is uncertain due to the lack of data. Regarding the following model calibration, we assume that the shale is fully saturated with kerogen at wells 1 and 3.

The kinetic reaction corresponding to smectite/illite conversion assumes $E = 39 \text{ kcal/mol}$ and $A = 1.217 \times 10^{23} / \text{m.y.}$ (Pytte and Reynolds, 1989). We consider that at a 1.8-km depth, the smectite/illite ratio is $r_0 = 0.99$. The kinetic-reaction parameters have been obtained by matching the log bulk density with the theoretical expression of the bulk density (see Figure 8b below). The conversion ratio is shown in Figure 5. As can be seen, smectite and illite are the main components at wells 1 and 3, respectively. The elastic properties of smectite and illite are given in Table 1 (Carcione, 2000; Totten et al., 2002; Carcione et al., 2011; Pinna et al., 2011). Due to compaction effects (closing of micropores), we assume that the density of kerogen is 1.2 g/cm^3 at well 1 and 1.3 g/cm^3 at well 3 (a simple calculation indicates a 1/13 volume reduction). The density of illite is an upper limit at very large confining pressures and can also be due the presence of pyrite and carbonates. Smectite is assumed to be isotropic, and its values have been taken from Wang et al. (2001). On the basis of the smectite and illite fractions given in Figure 5, we compute the P- and S-wave bedding-normal phase velocities and density $\rho_s = \rho_{sm} r + \rho_i (1 - r)$ of the mineral composing the frame, where ρ_{sm} and ρ_i are the densities of smectite and illite, respectively (Figure 6).

From well reports, we have precise values of TOC of the Spekk Formation at given depths (using a LECO CS244 carbon analyzer). In the following, we perform comparisons between the well-log data and model calculations at these depths. This first step constitutes the model calibration assuming that no liquid or gaseous hydrocarbons are present in the source rock. The volumetric kerogen content can be calculated in terms of the TOC (in weight percentage between 0 and 100) from

$$K = \frac{(\rho - \phi \rho_w) \text{TOC}}{C_k \rho_k (1 - \phi)}, \quad (6)$$

where ϕ is the porosity (water fraction in this case), ρ is the density of the source rock, ρ_k and ρ_w are the densities of kerogen and water, respectively, and C_k depends on the maturity level ranging from 0.7 to 0.85 (Vernik and Nur, 1992; Carcione, 2000; Vernik and Milovac, 2011). An alternative, simplified equation is given in Sondergeld et al. (2010), equation 12.

On the other hand, the bulk density in the absence of hydrocarbons is

$$\rho = \phi \rho_w + \phi_k \rho_k + (1 - \phi - \phi_k) \rho_s, \quad (7)$$

where $\phi_k = K/100$. Combining equations 6 and 7, we solve for porosity from

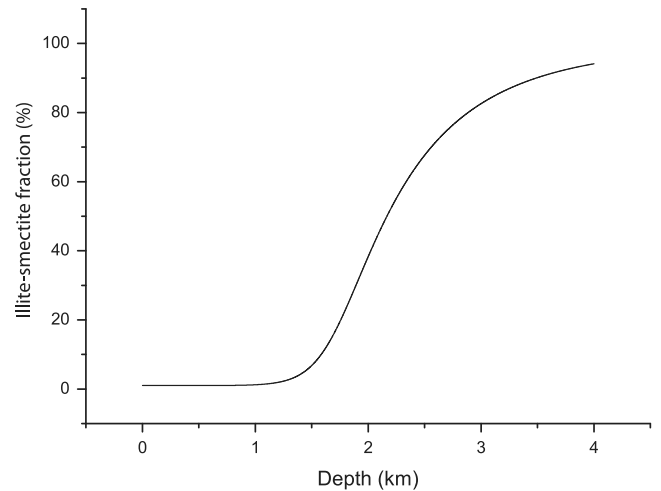


Figure 5. Illite/smectite ratio as a function of depth.

Table 1. Material properties.

Medium	Depth (km)	V_{11} (km/s)	V_{33} (km/s)	V_{55} (km/s)	V_{66} (km/s)	V_{13} (km/s)	ρ (g/cm ³)
Smectite	—	2.8	2.8	1.7	1.7	1.43	2.2
Illite	—	5	4.5	2.9	3.15	1.96	2.9
Kerogen ³	2	2.327	2.327	1.5	1.5	0.96	1.2
Kerogen ³	3	2.236	2.236	1.44	1.44	0.92	1.3
Water	2	1.66	1.66	0	0	1.66	1.04
Water	3	1.65	1.65	0	0	1.65	1.02
Smectite-illite-water	2	3.84	2.88	1.68	2.38	1.48	2.38
Smectite-illite-water	3	4.73	3.80	2.37	2.97	1.72	2.75
Oil	3	1.11	1.11	0	0	1.11	0.73
Gas	3	0.82	0.82	0	0	0.82	0.14

³Here, $K_k = 2.9 \text{ GPa}$ and $\mu_k = 2.7 \text{ GPa}$ (Mavko et al., 2009).

$$\begin{aligned}
 A\phi^2 + B\phi + C &= 0, \\
 A &= \rho_s - \rho_w, \\
 B &= \rho + \rho_w(1 - a\rho_k + a\rho_s) - 2\rho_s, \\
 C &= \rho_s + \rho(a\rho_k - a\rho_s - 1), \\
 a &= \frac{\text{TOC}}{C_k\rho_k},
 \end{aligned}
 \tag{8}$$

and for kerogen content from equation 6. The bulk density ρ is obtained from the density logs. We assume $C_k = 0.75$, $\rho_w = 1.04 \text{ g/cm}^3$ (well 1), and $\rho_w = 1.02 \text{ g/cm}^3$ (well 3) (see Figure 17 below). TOC and K are represented in Figure 7 as a function of depth, where the average values of K are approximately 14% and 26% in wells 1 and 3, respectively.

The density of the shale mineral is shown in Figure 6b, and the porosity from equation 8 is used to calculate the bulk density of the shale (equation 7), where the kerogen content values are obtained from equation 6. Figure 8 shows (a) the porosity derived from equa-

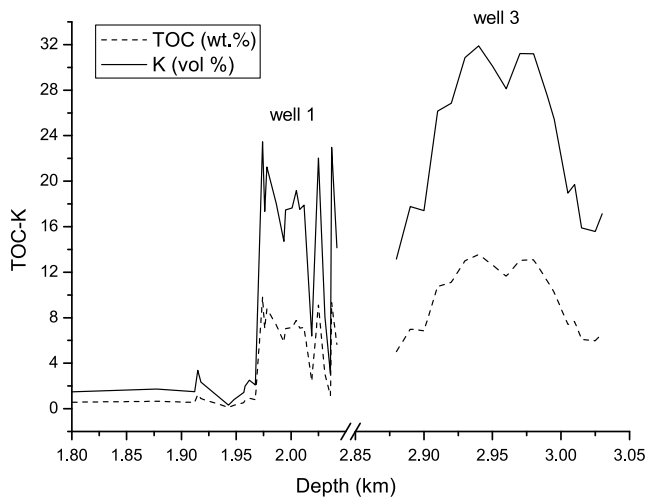


Figure 7. TOC (in weight percent) and kerogen content K (in volume percent) corresponding to wells 1 and 3.

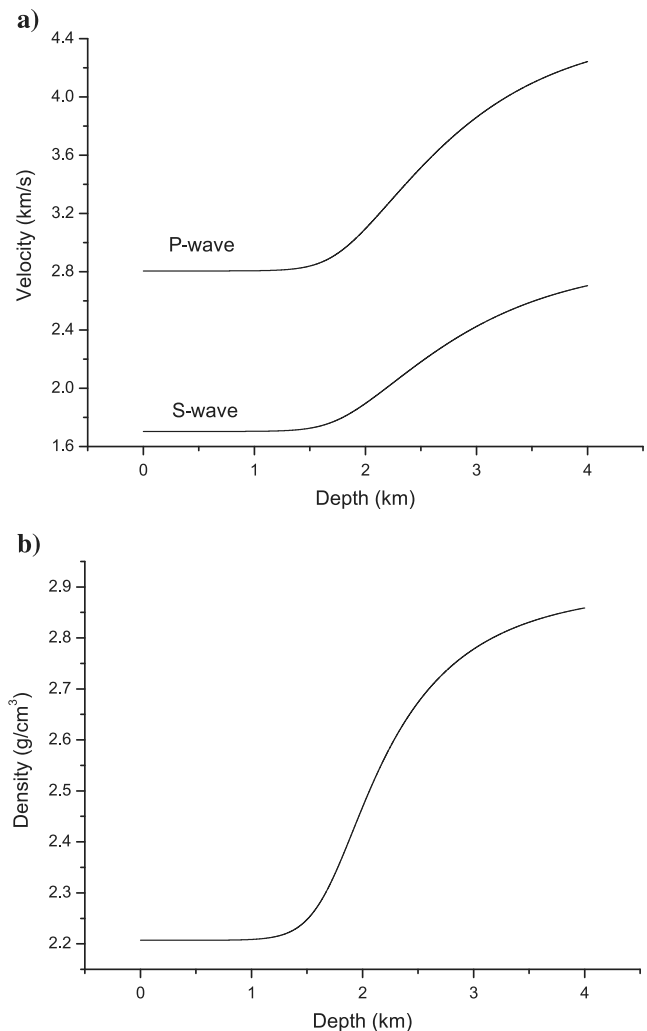


Figure 6. (a) Phase-velocity variations (V_{33} [P-wave] and V_{55} [S-wave]) and (b) mass density of the mineral composing the shale frame as a function of depth due to diagenesis (smectite/illite conversion).

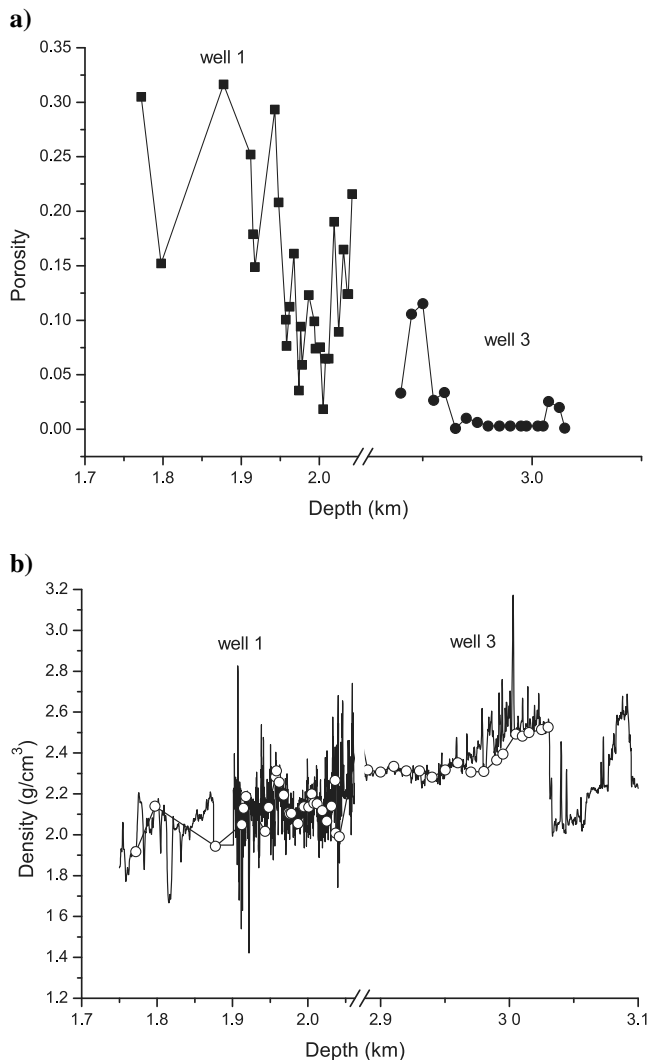


Figure 8. (a) Porosity and (b) bulk density as a function of depth corresponding to wells 1 and 3. The open circles correspond to calculations performed with the properties given in Table 1.

tion 8 and (b) the bulk density calculated from equation 7 (open circles) compared with the log bulk density (solid line). As can be appreciated, the comparison is satisfactory.

Alternatively, TOC has been expressed as a function of rock density by an empirical relations in Vernik and Landis (1996) and Carcione (2000) as

$$\text{TOC (wt.\%)} = 67 \frac{\rho_k(\rho_s - \rho)}{\rho(\rho_s - \rho_k)}, \quad (9)$$

where TOC accounts for approximately 67% of the bulk kerogen. A comparison to the TOC values given in the well reports is shown in Figure 9, showing a relatively good agreement.

Next, we compute the bedding-normal P-wave velocities V_{33} of the shale using Backus averaging and the Gassmann equation (Carcione et al., 2011). We assume that water is saturating the mineral material composed of smectite and illite, and we use the Gassmann equation to obtain the elasticity constants of the mineral/water composite medium. In this case, the pore infill is water (its shear modulus is set to a small value in order for the equation to work). The equations to obtain the elasticity constants of this composite medium require the dry-rock elasticity constants, which are obtained from equation C-2 with $A = 1.5$ and $B = 4$ (Appendix C). Likewise, the same parameters are used to obtain the dry-rock elasticity constants required by the Gassmann equation to compute the elasticity constants of the shale saturated with kerogen. Figure 10 shows the bedding-normal P-wave velocities as a function of depth. The solid lines and open circles correspond to the sonic-log data and model calculations, respectively. The agreement is very good, with Backus averaging and Gassmann equations giving similar results for well 3. Figure 11 compares data and model calculations of the bedding-normal S-wave velocity V_{55} . The agreement in the depth range, where the TOC values are known is acceptable. The anisotropy parameters 4 are shown in Figure 12, where strong anisotropy can be observed. Parameter δ is negative in all the cases (the P-wave velocity increases away from the vertical, if δ is positive and decreases if δ is negative). The Backus model predict more anisotropy than the Gassmann model. The agreement is intended in average with a uniform set of parameters (properties) along the well. A point-to-point match would require to use different set of parameters at each log depth, and this is meaningless considering that we have to retrieve the amount of organic matter (kerogen content, presence of fluids, and possible overpressure) from seismic data that have lower resolution. The agreement is “satisfactory” in this sense.

For comparison, we show in Figure 13 the sonic, density, and gamma-ray logs. Higher velocities in well 2 indicate that the amount of kerogen in this well can be much lower than that in well 3 in the studied range (2.9- to 3.05-km depth). This fact is also reflected in the bulk density and gamma-ray logs, with lower and higher values in well 3, respectively. High kerogen content in well 2 can be hypothesized in the range 2.6–2.8 km depth, where the P-wave velocity and bulk density show low values and the gamma ray has high values. The previous analysis and these results support the fact that at the calibration wells, mainly kerogen is present because the models match the data without including fluids other than water. Figures 14 and 15 show the fit of the Spekk Formation in well 3, where the symbols correspond to the model predictions (Backus averaging). The Gassmann equations provide a similar agreement.

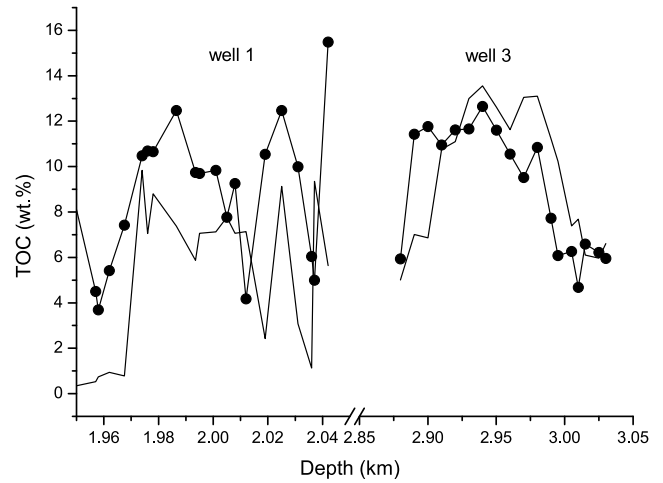


Figure 9. The TOC (in weight percent) from well reports (solid line) and predicted by equation 9 (full circles), corresponding to wells 1 and 3.

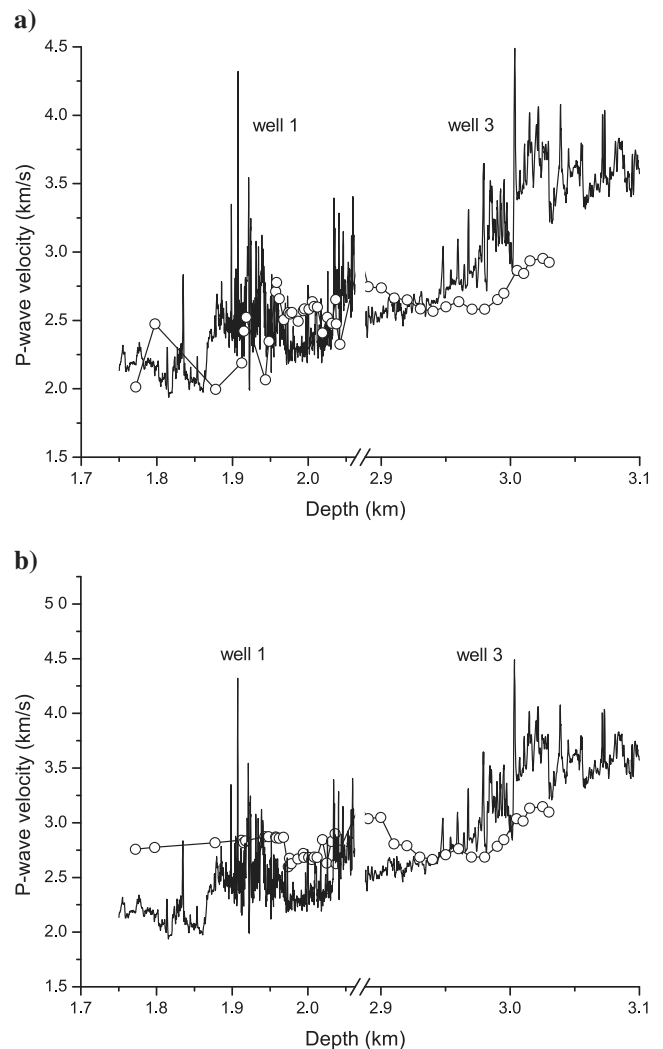


Figure 10. (a) Backus and (b) Gassmann bedding-normal P-wave velocities as a function of depth, corresponding to wells 1 and 3. The solid lines and open circles correspond to the well-log data and model calculations at the depths indicated at the well reports, respectively.

Figure 16 illustrates the calibration process. Basically, the TOC values, as well as the density and sonic logs are used. Additional information is required, such as the sedimentation history of the area.

ROCK-PHYSICS TEMPLATES

The properties of the fluids depend on depth, temperature, and pore pressure. The hydrostatic pore pressure is $p_H = \bar{\rho}_w g z$, where $\bar{\rho}_w = 1.04 \text{ g/cm}^3$, the brine salinity is $s_c = 100,000 \text{ ppm}$, the oil API gravity is 50, and the geothermal gradient is $G = 37^\circ\text{C/km}$. To build the templates, we assume similar conditions as those given in well 3, where the presence of oil and gas is more probable. We then consider a depth of 3 km, that the mineral forming the frame of the shale (smectite-illite-water) has 5% water ($\phi_w = 0.05$) and that the kerogen fraction can reach a maximum value of 30% ($\phi_k = 0.3$). The kerogen properties are defined by $K_k = 6.6 \text{ GPa}$, $\mu_k = 2.7 \text{ GPa}$,

and $\rho_k = 1.4 \text{ g/cm}^3$ (Carcione, 2000; Carcione et al., 2011; Pinna et al., 2011).

We assume that the pore pressure has been released and remains hydrostatic; otherwise, the pressure effect on the rock frame has to be considered (this effect is modeled below). Under these conditions, the mineral properties (including water) and the fluid properties are given in Table 1. To obtain the bulk modulus of the oil-gas mixture, we consider the mesoscopic-loss theory developed in Appendix B (equation B-5). This attenuation mechanism affects the seismic velocity depending in the size of the gas patches. Figure 17 shows the bulk modulus as a function of frequency for different values of the gas-pocket radius, r_0 ($\varphi = 0.3$ is assumed). The Wood average, which is normally used, is also shown. We consider $r_0 = 1 \text{ cm}$ in the following calculations.

The proportion of the kerogen-oil-gas mixture is $\phi_k + \phi_f = \phi_k + \phi_o + \phi_g$, and the proportion of solid to water is $\phi_s + \phi_w$, where *solid* stands for the smectite-illite mixture. The porosity is

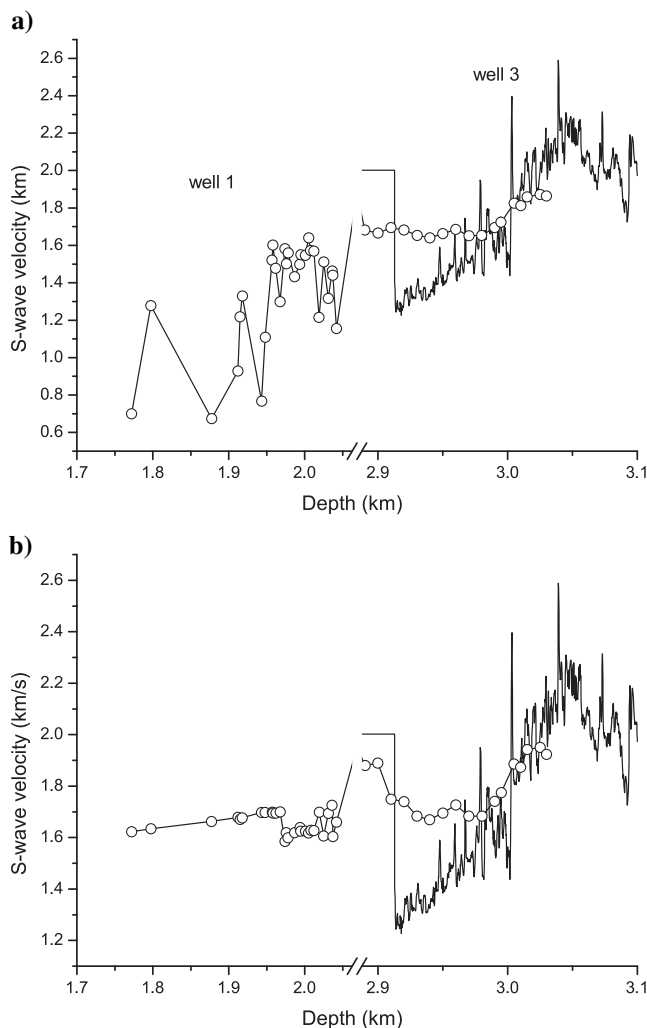


Figure 11. Bedding-normal S-wave velocity as a function of depth, corresponding to (a) Backus averaging and (b) the Gassmann equation. The solid lines and open circles correspond to the well-log data and model calculations at the depths indicated at the well reports, respectively.

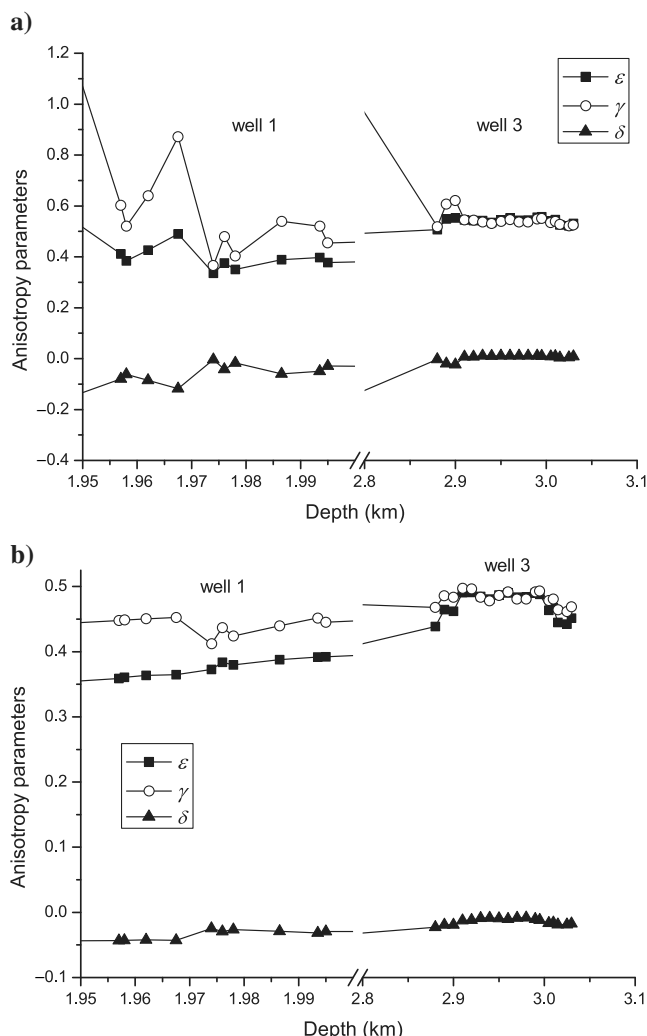


Figure 12. Anisotropy parameters as a function of depth obtained from the (a) Backus and (b) Gassmann models, corresponding to wells 1 and 3, at the depths where TOC is given in the well reports.

$\phi = \phi_w + \phi_o + \phi_g$, and we have $\phi_s + \phi_w + \phi_k + \phi_o + \phi_g = 1$. Backus averaging “mixes” the kerogen-oil-gas and the solid-water phases with the respective proportion indicated above. We define the oil and gas saturation as $S_o = \phi_o/\phi$ and $S_g = \phi_g/\phi$, respectively,

and the kerogen content is $K = 100\phi_k$. In what follows, we fix the amount of organic content, defined by $\phi_{OC} = \phi_k + \phi_o + \phi_g$ and vary the kerogen, oil, and gas proportions. It is $\phi_{OC} + \phi_w + \phi_s = 1$. Summarizing, we have the set of relations

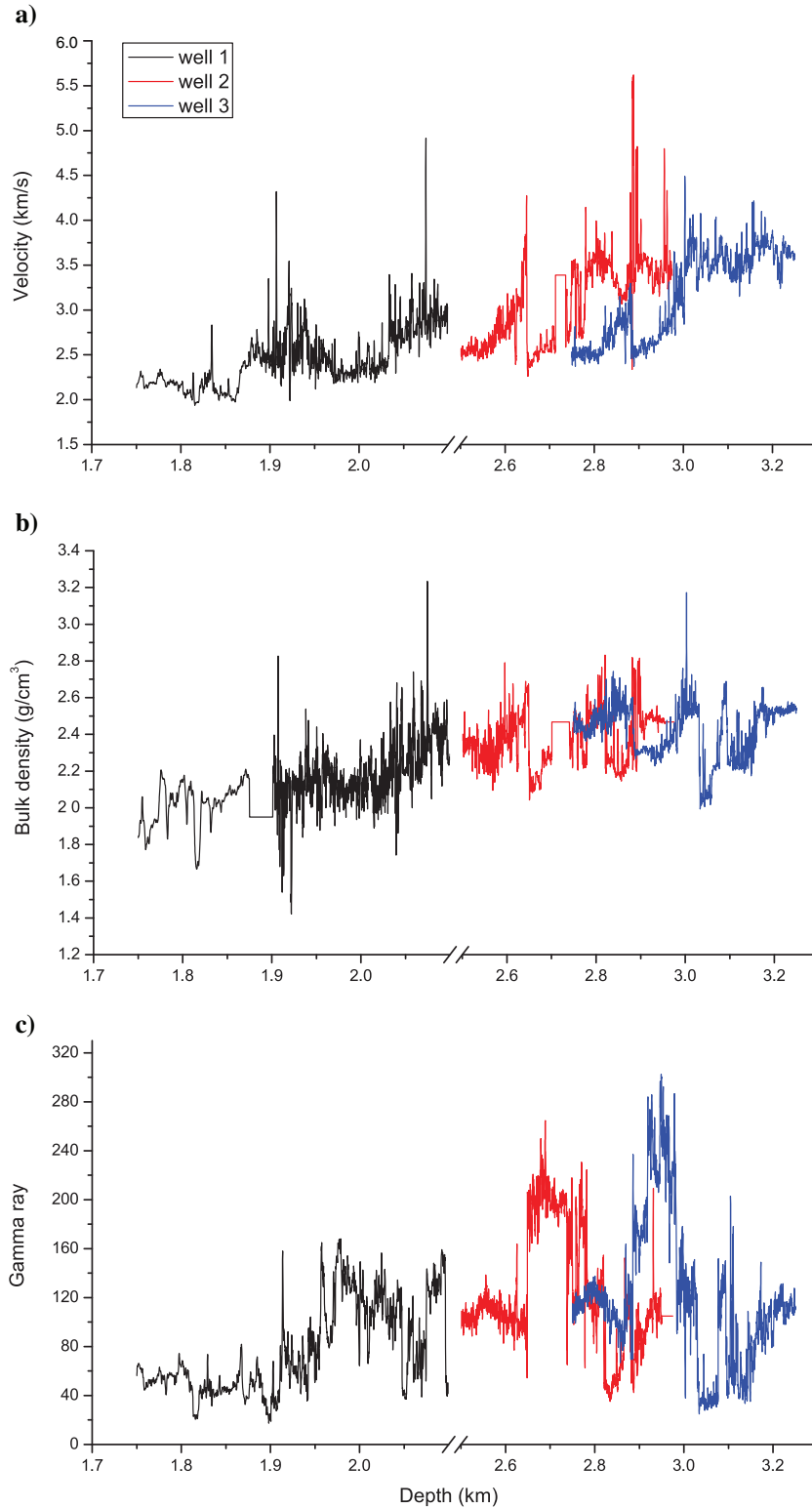


Figure 13. Sonic, density, and gamma-ray logs.

$$\begin{aligned}
 \phi_{OC} &= \phi_k + \phi_o + \phi_g, \\
 \phi &= \phi_w + \phi_o + \phi_g, \\
 S_w &= \phi_w / \phi, \\
 S_o &= \phi_o / \phi, \\
 S_g &= \phi_g / \phi, \\
 \phi_{OC} + \phi_w + \phi_s &= 1, \\
 \phi_o &= S_o(\phi_{OC} + \phi_w - \phi_k), \\
 \phi_g &= S_g(\phi_{OC} + \phi_w - \phi_k),
 \end{aligned}
 \tag{10}$$

and all the quantities greater than zero. The correction to the bedding-parallel stiffness constants of the mixture solid-water when using

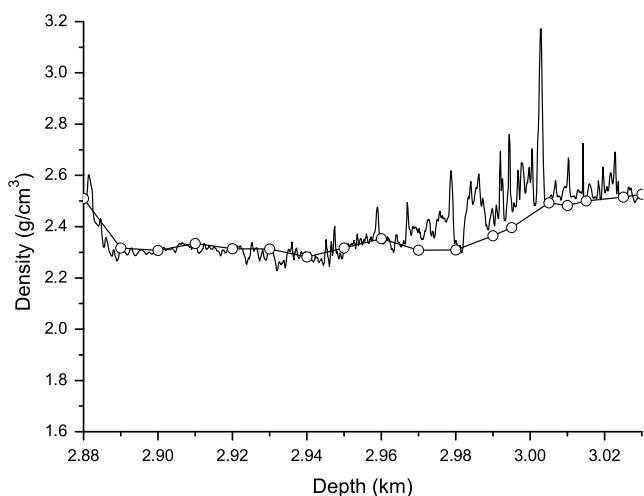


Figure 14. Bulk density from (a) logs and (b) theory, corresponding to an smectite/illite activation energy of 39 kcal/mol and a smectite density of 2.2 g/cm³.

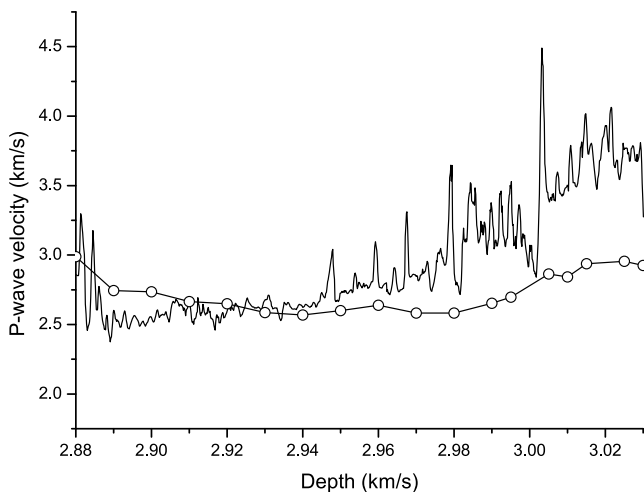


Figure 15. Bedding-normal P-wave velocity from (a) logs and (b) theory, corresponding to an smectite/illite activation energy of 44 kcal/mol and a smectite density of 2.6 g/cm³.

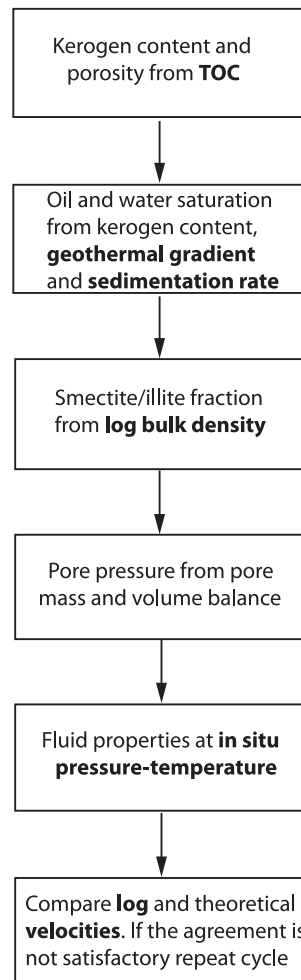


Figure 16. Calibration flowchart. The main data used for the calibration are indicated in bold font.

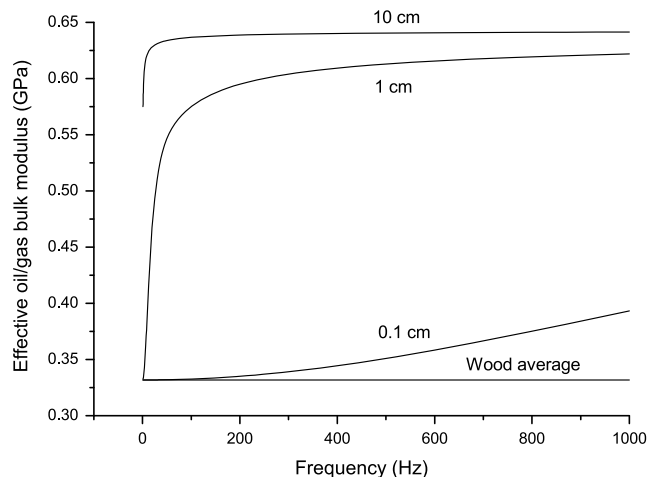


Figure 17. The effective bulk modulus of the oil-gas mixture as a function of frequency due to the mesoscopic-loss mechanism. The Wood average is also shown.

Backus averaging is not applied here because it is unstable in the presence of fluids (it gives negative stiffness constants). The density of the kerogen-oil-gas mixture is $\rho_{OC} = (\phi_k \rho_k + \phi_o \rho_o + \phi_g \rho_g) / \phi_{OC}$, and the bulk density is $\rho = (1 - \phi_{OC}) \bar{\rho}_s + \phi_{OC} \rho_{OC}$, where $\bar{\rho}_s = (\phi_s \rho_s + \phi_w \rho_w) / (\phi_s + \phi_w)$ is the density of the smectite-illite-water mixture.

Figures 18 and 19 show the (a) bedding-normal and (b) bedding-parallel P-wave velocities as a function of gas saturation for various values of the kerogen content and oil saturation. The models are Backus averaging and the Gassmann equation, respectively, and the frequency is 50 Hz. Both models behave similarly at full kerogen saturation, as we have previously seen, but they predict different behaviors in the presence of fluids, mainly the velocities along the bedding plane. The velocities decrease with decreasing kerogen content, but they may increase or decrease as a function of oil and gas saturations due to the density effect. Backus averaging predicts very low normal-bedding velocities at $K = 0\%$, and high-bedding parallel velocities, indicating that this model provides lower and upper limits (Carcione et al., 2011).

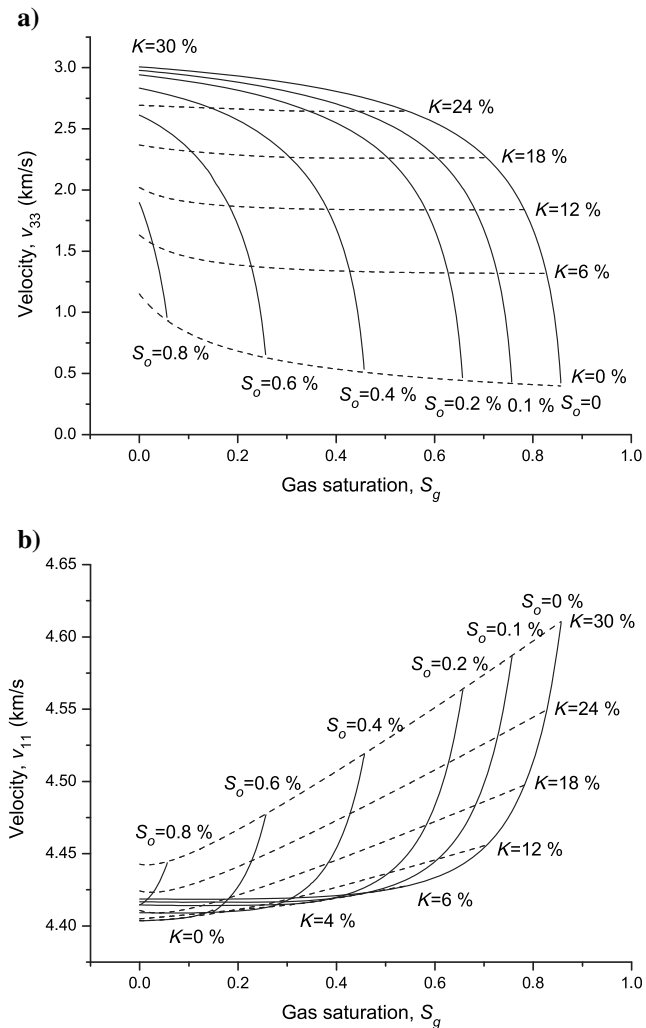


Figure 18. (a) Bedding-normal and (b) bedding-parallel P-wave velocities as a function of gas saturation S_g for various values of the kerogen content $K = 100\phi_k$, and oil saturation S_o (dashed and solid lines, respectively). The model is Backus averaging, and the frequency is 50 Hz.

The energy velocities for a shale with (a) full kerogen content (immature) and (b) a shale saturated with oil and gas (mature) are shown in Figure 20. The depth is 3 km, $\phi_w = 0.05$, the model is the Gassmann equation, and the frequency is 50 Hz. In the first case, $K = 0.3$, $S_o = S_g = 0$, $\bar{c}_{11} = 37.3$ GPa, $\bar{c}_{13} = 6.21$ GPa, $\bar{c}_{33} = 22.33$ GPa, $\bar{c}_{55} = 7.70$ GPa, $\bar{c}_{66} = 14.04$ GPa, and $\bar{\rho} = 2347$ kg/m³; in the second case, it is $K = 0$, $S_o = 0.7$, $S_g = 0.15$, $\bar{c}_{11} = 29$ GPa, $\bar{c}_{13} = 1.64$ GPa, $\bar{c}_{33} = 6$ GPa, $\bar{c}_{55} = 2$ GPa, $\bar{c}_{66} = 11$ GPa, and $\bar{\rho} = 2113$ kg/m³. The presence of fluids has decreased substantially the velocities and induced considerable S-wave splitting.

In the following templates (Figures 21–23), we maintain constant the water and organic-matter fractions $\phi_w = 0.05$ and $\phi_{OC} = 0.2$, respectively. Figures 21 and 22, respectively, show V_P/V_S as a function of the acoustic impedance (AI) and $\lambda - \mu - \rho$ templates for various values of the gas and oil saturation (solid and dashed lines, respectively). The models are (a) Backus averaging and (b) the Gassmann equation; the minimum amount of kerogen is 5%, and the frequency is 50 Hz. The Wood average to obtain the bulk modulus of the fluid mixture has been used here because the results

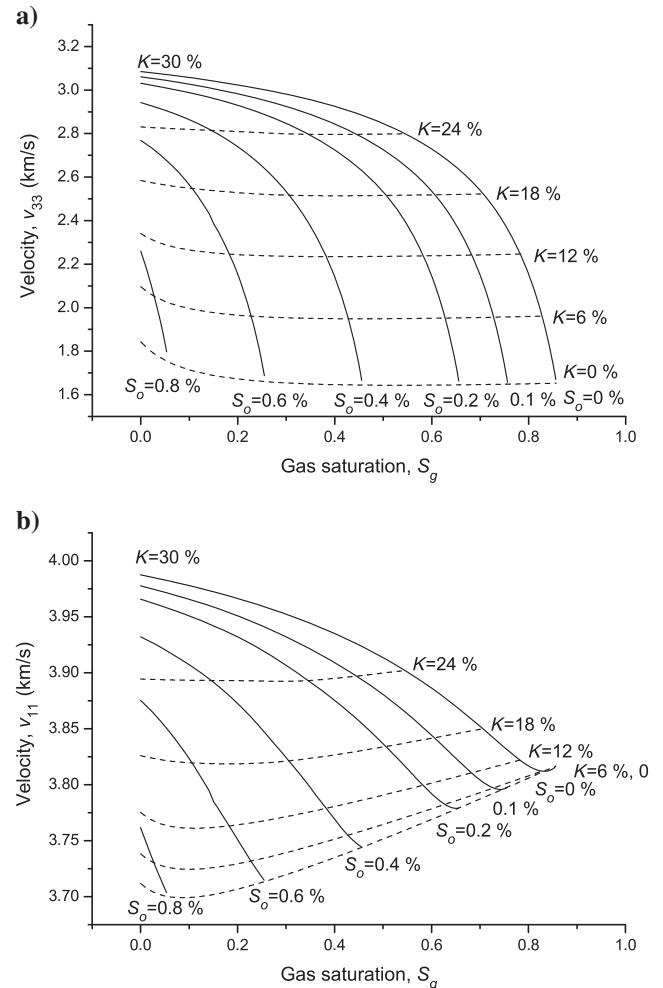


Figure 19. (a) Bedding-normal and (b) bedding-parallel P-wave velocities as a function of gas saturation for various values of the kerogen content and oil saturations (see Figure 17). The model is the Gassmann equation, and the frequency is 50 Hz.

are similar to those of the White model. Given the values of S_g and S_o , the kerogen content is

$$K = 100\phi_k = 100 \frac{\phi_{OC} - (S_o + S_g)(\phi_{OC} + \phi_w)}{1 - S_o - S_g}. \quad (11)$$

In both cases, the main variations occur at low gas saturations and high oil saturations, with the Gassmann equation predicting lower V_p/V_s values, whereas the $\lambda - \mu - \rho$ templates are very similar. The $Y - \nu$ (Young modulus/Poisson ratio) templates are shown in Figure 23 for the three Poisson ratios defined in equation 3. The Young modulus is defined in equation 5, and the rock-physics model is Backus averaging.

To build templates of the elastic properties at different pore pressures, we have to establish a proper model in agreement with experimental data. The pore-pressure effects are modeled with the equations given in Carcione et al. (2011) and Pinna et al. (2011), where we assume that the dry-rock elasticity constants of the smectite-illite frame (without the water) are affected by the confining and pore pressures. Invoking the effective pressure law (Carcione, 2001a, 2001b; Gei and Carcione, 2003) and assuming that the effective pressure is equal to the differential pressure $p_d = p_c - p$, where p is the pore pressure, the confining pressure can be replaced by the differential pressure.

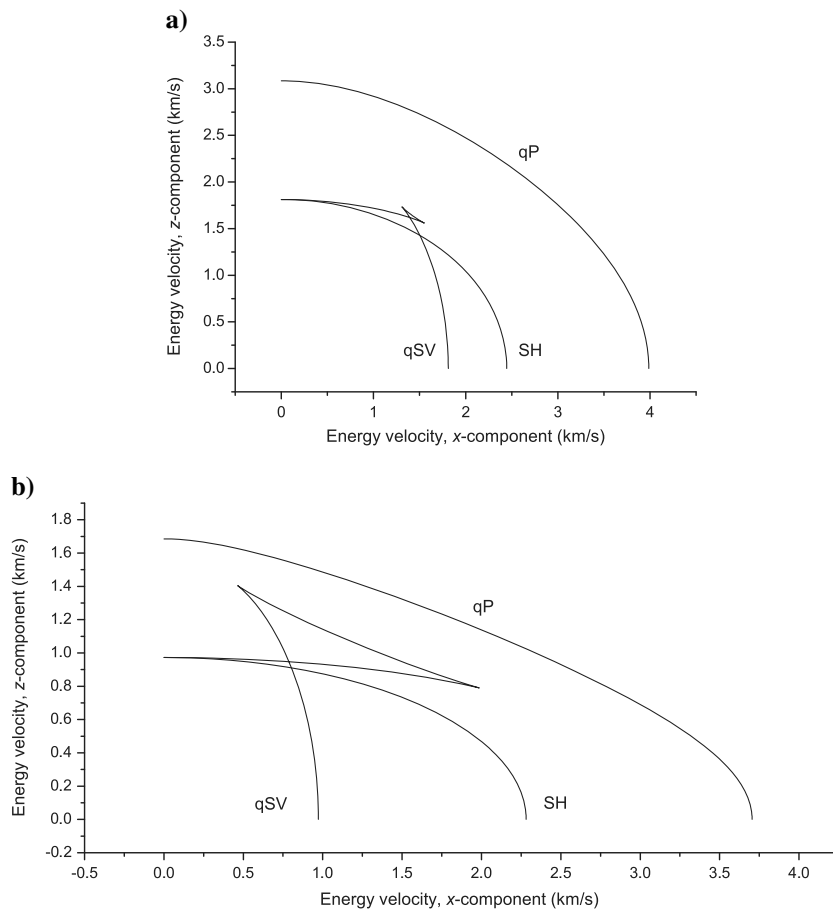
We consider the inverse Gassmann equation (Carcione et al., 2011), which can be implemented if detailed laboratory data are available. This approach can also be used to perform fluid substi-

tution. To illustrate the method, we consider a sample of Kimmeridge Shale fully saturated with kerogen, taken from a depth of 2768 m, whose velocities are given in Table 2 (see Tables A-1 and A-4 in Vernik, 1995; angles (0) and (90) correspond to pairs “33” and “11” (P-waves) and “55” and “66” (S-waves) in Table 1). This sample is strongly anisotropic, with $\epsilon = 0.35$ and $\gamma = 0.33$. Based on a grain density $\bar{\rho}_s = 2.17 \text{ g/cm}^3$ and kerogen properties $V_p = 2.6 \text{ m/s}$, $V_s = 1.2 \text{ m/s}$, $\rho_k = 1.4 \text{ g/cm}^3$, the wet-rock elasticity constants are given in Table 2. The kerogen content is $K = 40\%$, and the bulk density is $\rho = 1.862 \text{ g/cm}^3$ (Vernik, 1995). The inversion yields the dry-rock elasticity constants reported in Table 2. The elasticity constants of the smectite-illite-water composite (assumed isotropic) used for the inversion are $c_{33}^s = 16.5 \text{ GPa}$ and $c_{55}^s = 5.5 \text{ GPa}$, corresponding to a Poisson medium with $V_p = 2.76 \text{ km/s}$, $V_s = 1.593 \text{ km/s}$, and $\bar{\rho}_s = 2.17 \text{ g/cm}^3$ (this medium has the two Lamé constants equal). This choice satisfies the stability conditions. As can be seen in Table 2, the elasticity constants c_{33}^m and c_{55}^m , related to the direction perpendicular to layering, are more affected by changes in the confining pressure, particularly c_{33}^m , whose value is much lower than the wet-rock value. This is due to the high kerogen content as shown by Carcione et al. (2011), who obtained dry-rock elasticity constants for various samples of the Bakken shale.

Using the procedure given in Carcione et al. (2011), we obtain

$$c_{IJ}^m = \hat{c}_{IJ} + \check{c}_{IJ} \exp(-p_d/p_{IJ}^*), \quad (12)$$

Figure 20. Energy velocity for a shale with (a) full-kerogen content (immature) and (b) a shale saturated with oil and gas (mature). The model is the Gassmann equation, and the frequency is 50 Hz.



where $p_d = p_c - p_H$ and

$$\begin{aligned} \hat{c}_{11} &= 19.72 \text{ GPa}, & \check{c}_{11} &= -0.67 \text{ GPa}, & p_{11}^* &= 17.73 \text{ MPa}, \\ \hat{c}_{13} &= 5.54 \text{ GPa}, & \check{c}_{13} &= -0.88 \text{ GPa}, & p_{13}^* &= 22.10 \text{ MPa}, \\ \hat{c}_{33} &= 15.98 \text{ GPa}, & \check{c}_{33} &= -18.81 \text{ GPa}, & p_{33}^* &= 15.72 \text{ MPa}, \\ \hat{c}_{55} &= 4.40 \text{ GPa}, & \check{c}_{55} &= -1.24 \text{ GPa}, & p_{55}^* &= 27.64 \text{ MPa}, \\ \hat{c}_{66} &= 6.87 \text{ GPa}, & \check{c}_{66} &= -0.52 \text{ GPa}, & p_{66}^* &= 19.43 \text{ MPa}. \end{aligned} \quad (13)$$

One could consider the smectite/illite conversion and kerogen/oil/gas generation and the induced pore pressure affecting the rock properties, but the objective is to analyze the elastic properties of the shale for varying pore pressure and fixed values of the kerogen content and oil and gas saturations. We then assume that a rock at a given depth is subject to pore-pressure changes. In this case, the stiff porosity is constant and pressure affects mainly the dry-rock moduli by closure of microcracks, whose (soft) porosity is negligible compared with the stiff porosity. In a lesser degree, pressure also affects the bulk density, mainly through the gas density. We

consider the dry-rock elasticity constants (equation 12) and the parameterization of equation 13, representing the rock frame made of the smectite-illite-water composite “mineral.” The depth of this shale is 2768 m, and the hydrostatic and confining pressures are $p_H = 28$ and $p_c = 68$ MPa, respectively. Based on the density of the smectite-illite-water composite (2.17 g/cm^3) and assuming a proportion of illite of 76% (according to Figure 5), the smectite-illite density is 2.74 g/cm^3 , giving a water proportion $\phi_w = 0.2$. We assume $S_o = 0.3$ and $S_g = 0.1$ and because $\phi_{OC} = 0.4$ and using equations 10 and 11, we have $\phi_k = 0.27$ ($K = 27\%$), $\phi_o = 0.1$, and $\phi_g = 0.033$. Figure 24 shows the dry-rock and wet-rock velocities as a function of the differential pressure ($p_d = p_c - p$) for full kerogen content and (a) $S_o = 0.3$ and (b) $S_g = 0.1$. The bedding-normal P-wave velocity is highly affected by the pore pressure and the presence of fluids. The dry-rock velocities are generally higher due to the density effect.

It is clear that the replacement of kerogen by a lower density material (oil or gas) greatly affects the bedding-normal P-wave modu-

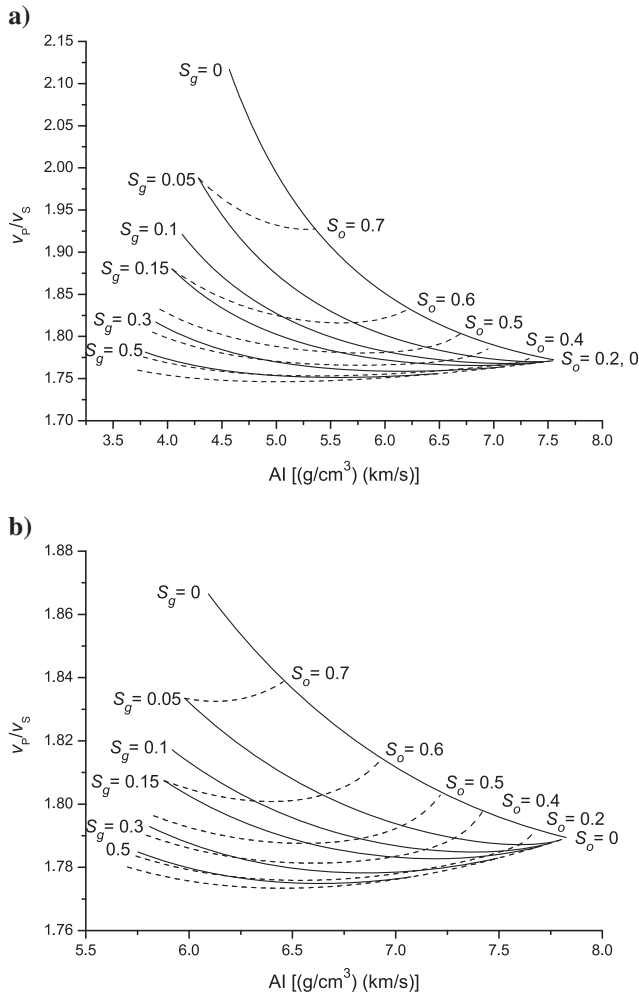


Figure 21. The V_P/V_S (v_{33}/v_{55}) as a function of the AI for various values of the gas and oil saturations (solid and dashed lines, respectively). The models are (a) Backus averaging and (b) the Gassmann equation, and the frequency is 50 Hz.

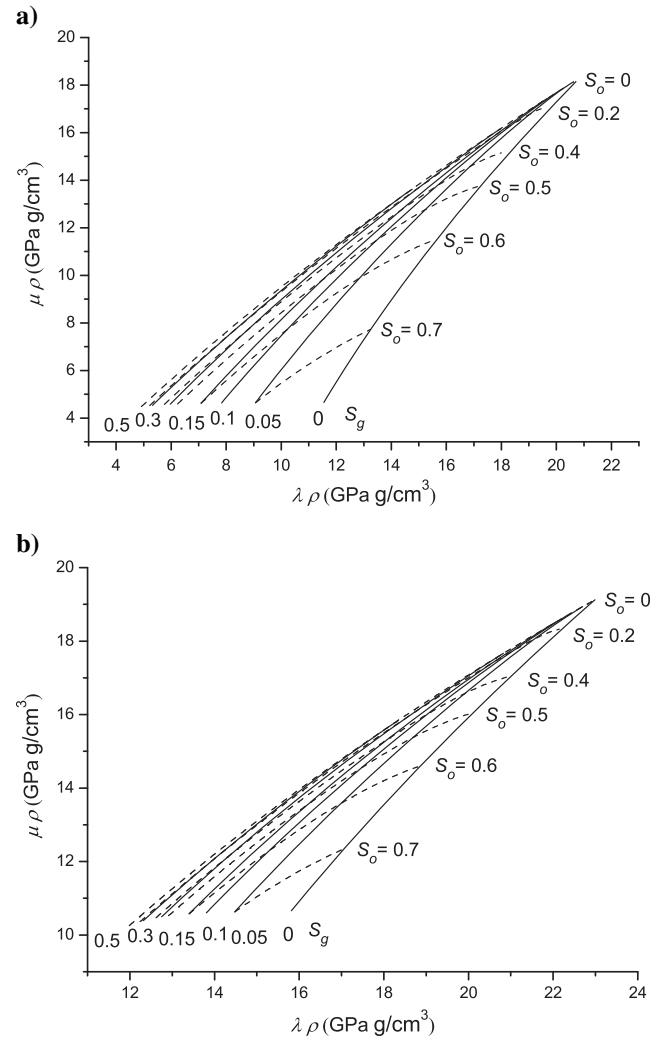


Figure 22. The $\lambda - \mu - \rho$ templates for various values of the gas and oil saturations (solid and dashed lines, respectively). The models are (a) Backus averaging and the (b) Gassmann equation, and the frequency is 50 Hz.

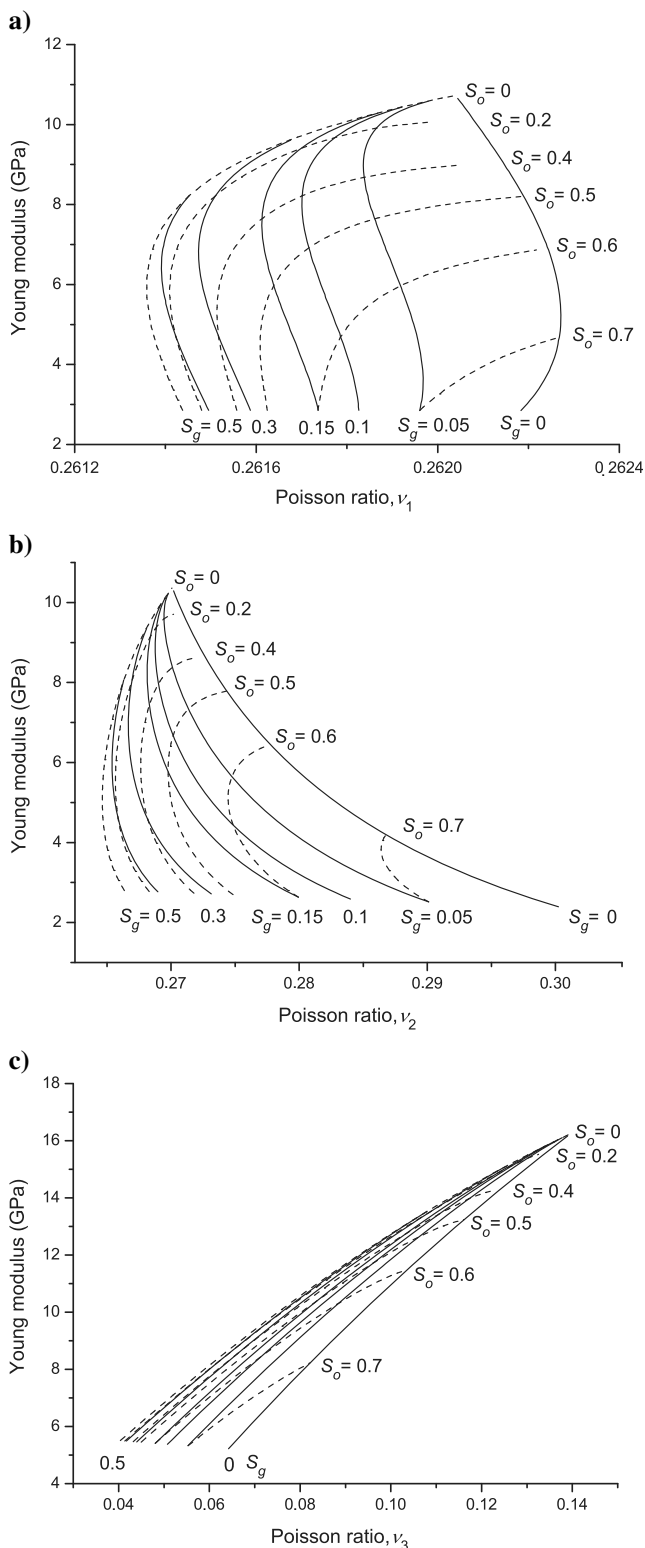


Figure 23. (a-c) The $Y - \nu$ (Young modulus/Poisson ratio) templates for various values of the gas and oil saturations (solid and dashed lines, respectively) and three definitions of the Poisson ratio. The model is Backus averaging.

lus. Next, we build templates for different pore pressures and varying oil saturation, assuming no gas. For a given oil saturation S_o , the kerogen content is $K = 100[\phi_{OC} - S_o(\phi_{OC} + \phi_w)]/(1 - S_o)$, which has to be greater than zero. This happens for $S_o \leq \phi_{OC}/(\phi_{OC} + \phi_w) = 0.66$ in this case. We have $K = 40\%$ at $S_o = 0$ and $K = 10\%$ at $S_o = 0.6$. Figure 25 shows V_P/V_S (v_{33}/v_{55}) as a function of the (a) AI and (b) the $\lambda - \mu - \rho$ template for different values of the pore pressure and varying oil saturation. The model is the Gassmann equation, and the frequency is 50 Hz. Unlike the case of varying gas saturation (see Figures 21 and 22), the $\lambda - \mu - \rho$ template seems to discriminate the different pore pressures better than V_P/V_S versus AI.

Finally, we consider a transversely isotropic shale layer of thickness h at 2 and 3 km containing kerogen and gas embedded in a homogeneous isotropic shale without organic matter (see Figure 26). The elastic properties of the homogeneous medium (smectite-illite-water composite with $\phi_w = 0.05$) at 2-km depth are $c_{33}^s = 20.5$ GPa, $c_{55}^s = 6.2$ GPa, and $\bar{\rho}_s = 2.398$ g/cm³, according to the smectite/illite conversion considered above. It is $V_P = 2.92$ km/s and $V_S = 1.61$ km/s. We assume $h = 25$ m, smaller than the dominant wavelengths of the P- and S-waves, which are approximately 97 and 53 m, respectively, for a frequency of 30 Hz. The elastic properties of the smectite-illite-water composite ($\phi_w = 0.05$) of the source rock are $c_{11}^s = 35$ GPa, $c_{13}^s = 7.4$ GPa, $c_{33}^s = 20.5$ GPa, $c_{55}^s = 6.2$ GPa, $c_{66}^s = 11.9$ GPa, and $\bar{\rho}_s = 2.398$ g/cm³. According to Krief equations C-2 and an organic matter content $\phi_{OC} = 0.25$ (maximum value in Figure 7), the elastic properties of the frame are $c_{11}^m = 24.6$ GPa, $c_{13}^m = 2.9$ GPa, $c_{33}^m = 8.1$ GPa, $c_{55}^m = 2.5$ GPa, and $c_{66}^m = 8.4$ GPa.

The elastic properties of the homogeneous medium (smectite-illite-water composite with $\phi_w = 0.05$) at 3-km depth are $c_{33}^s = 35$ GPa, $c_{55}^s = 11$ GPa, and $\bar{\rho}_s = 2.691$ g/cm³, according to the smectite/illite conversion considered above. It is $V_P = 4.6$ km/s and $V_S = 3.6$ km/s. The dominant wavelengths of the P- and S-waves are approximately 153 and 120 m, respectively. The elastic properties of the smectite-illite-water composite ($\phi_w = 0.05$) of the source rock are $c_{11}^s = 57.3$ GPa, $c_{13}^s = 12.6$ GPa, $c_{33}^s = 35$ GPa, $c_{55}^s = 11$ GPa, $c_{66}^s = 19.5$ GPa, and $\bar{\rho}_s = 2.691$ g/cm³. According to the Krief equations (equation C-2) and an organic matter content $\phi_{OC} = 0.25$ (the maximum value in Figure 7), the elastic properties of the frame are $c_{11}^m = 40.1$ GPa, $c_{13}^m = 4.8$ GPa, $c_{33}^m = 13$ GPa, $c_{55}^m = 4.2$ GPa, and $c_{66}^m = 13.6$ GPa.

Regarding the pore infill material, the kerogen and gas properties are those given in Table 1 at a 3-km depth. For a given gas saturation S_o , the kerogen content is $K = 100[\phi_{OC} - S_g(\phi_{OC} + \phi_w)]/(1 - S_g)$, which has to be greater than zero. This happens for $S_g \leq \phi_{OC}/(\phi_{OC} + \phi_w) = 0.83$ in this case. Gas saturation can be defined as $S_g = \phi_g/(\phi_g + \phi_w)$ (the definition so far) or $S'_g = \phi_g/(\phi_g + \phi_k)$ if we consider the organic pore infill. They are related as $S'_g = \phi_w S_g / [\phi_{OC}(1 - S_g)] < 0.97$. Figure 27 shows the real part of the reflection and transmission coefficients at (a) 2 km and (b) 3 km for a frequency of 30 Hz and a saturation $S_g = 0.2$ (for this saturation $S'_g = S_g$). The intercept and gradient for various values of the gas saturation and kerogen content are given in Table 3, and the data are represented in Figure 28, where it is clear that in all the cases, the AVO is class IV (Castagna and Swan, 1997). Yenugu and Han (2013) obtain a class IV AVO, but they compute the seismic response of a single interface consisting of Bakken shale overlain by a

Table 2. Kimmeridge-shale properties at 2768-m depth (Vernik, 1995).

p_c (MPa)	V_P (0) (m/s)	V_P (45) (m/s)	V_P (90) (m/s)	V_S (0) (m/s)	V_S (90) (m/s)
5	2690	2890	3520	1490	1910
30	2820	3030	3680	1540	1990
70	2920	3150	3790	1570	2020
p_c (MPa)	\bar{c}_{11} (GPa)	\bar{c}_{33} (GPa)	\bar{c}_{13} (GPa)	\bar{c}_{55} (GPa)	\bar{c}_{66} (GPa)
5	23.1	13.5	3.1	4.1	6.8
30	25.2	14.8	3.8	4.4	7.4
70	26.8	15.9	5	4.6	7.6
p_c (MPa)	c_{11}^m (GPa)	c_{33}^m (GPa)	c_{13}^m (GPa)	c_{55}^m (GPa)	c_{66}^m (GPa)
5	19.2	2.3	4.8	3.3	6.5
30	19.6	13.1	5.3	4	6.8
70	19.7	15.8	5.5	4.3	6.9

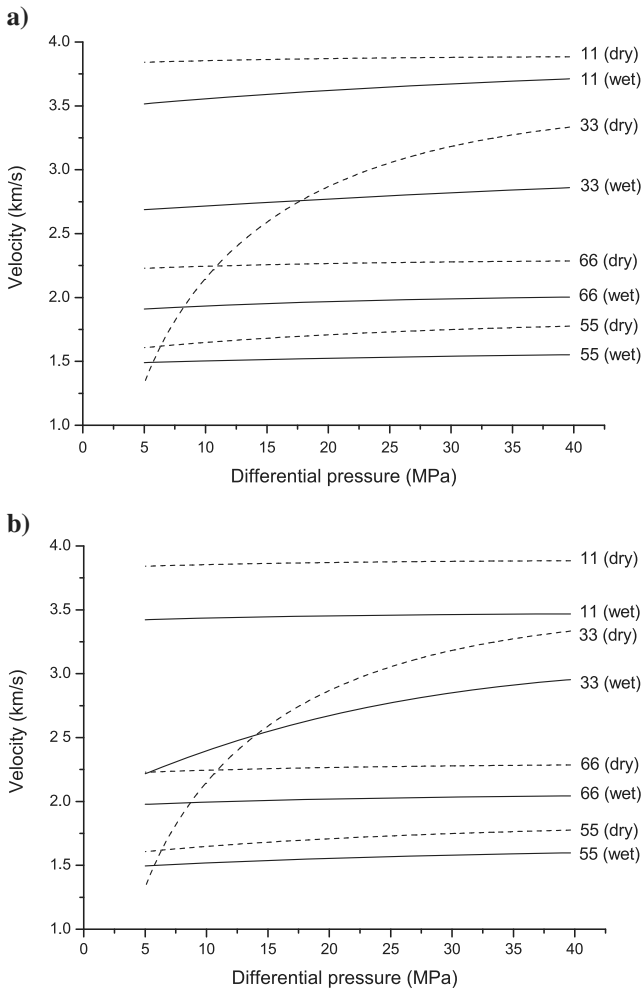


Figure 24. Dry-rock velocities (dashed lines) and wet-rock velocities (solid lines) as a function of the differential pressure for full kerogen and (a) $S_o = 0.3$ and (b) $S_o = 0.1$. The pairs 11 and 33, as well as 66 and 55 denote velocities along the horizontal and vertical directions, respectively.

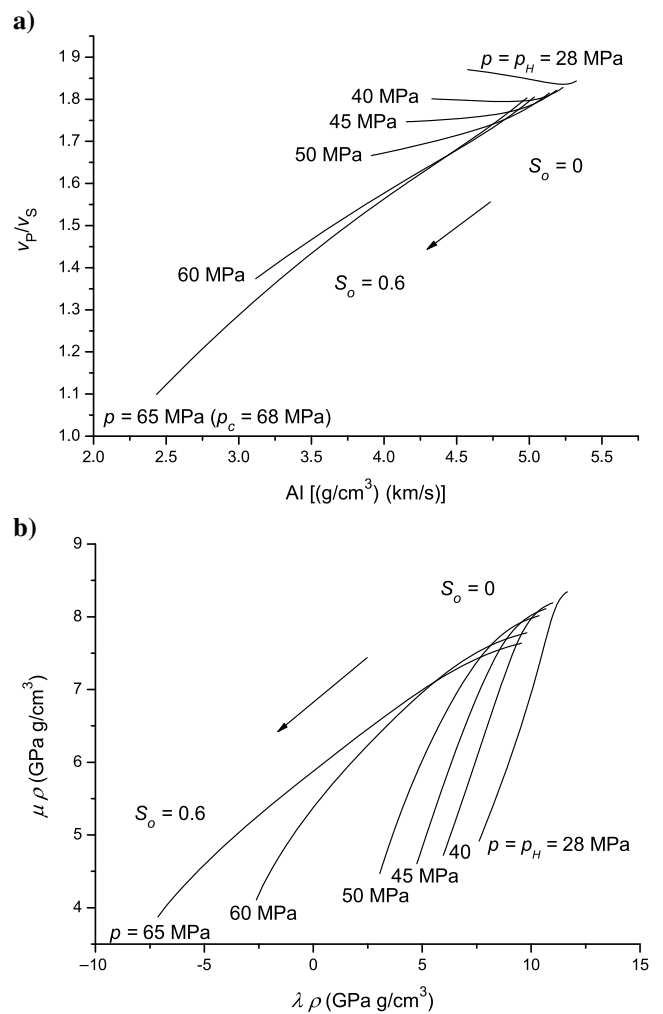


Figure 25. The V_P/V_S (V_{33}/V_{55}) as a function of the (a) AI and (b) $\lambda - \mu - \rho$ template for different values of the pore pressure and varying oil saturation. The model is the Gassmann equation, and the frequency is 50 Hz.

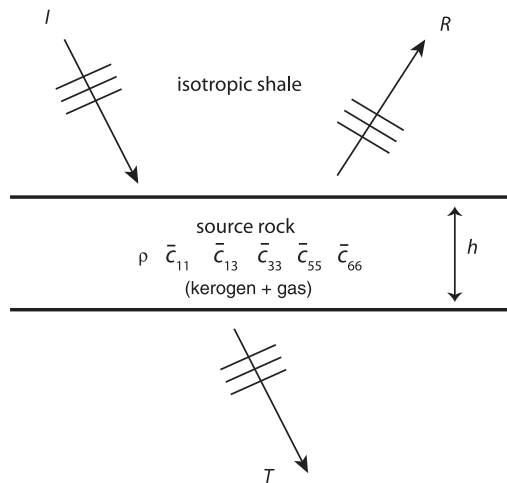


Figure 26. Source-rock layer to study the AVO effects of organic matter.

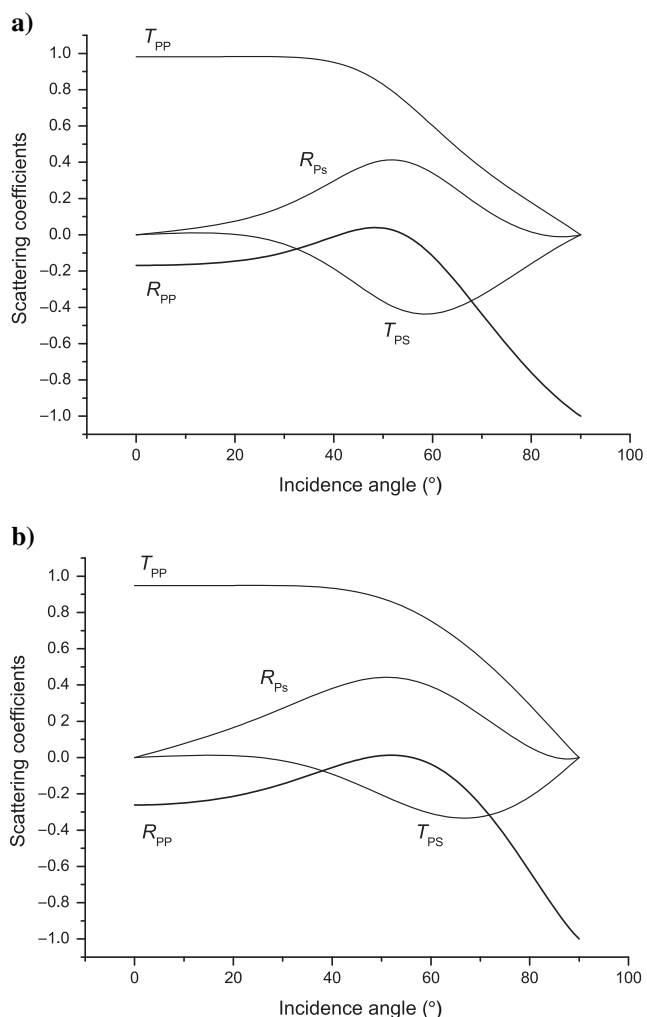


Figure 27. The real part of the reflection and transmission coefficients at depths of (a) 2 km and (b) 3 km, corresponding to a source-rock layer of $h = 15$ m (thickness) and gas saturation $S_g = 0.2$. The model is the Gassmann equation, and the frequency is 30 Hz.

Table 3. Intercept and gradient of a source-rock layer.

S_g	S'_g	K (%)	A	B
0	0	25	-0.24	0.42
0.1	0.02	24.4	-0.25	0.44
0.2	0.05	23.7	-0.26	0.48
0.3	0.08	22.8	-0.27	0.49
0.4	0.13	21.6	-0.29	0.51
0.5	0.2	20	-0.32	0.52
0.6	0.3	17.5	-0.35	0.54
0.7	0.46	13.3	-0.4	0.55
0.8	0.8	5	-0.48	0.56

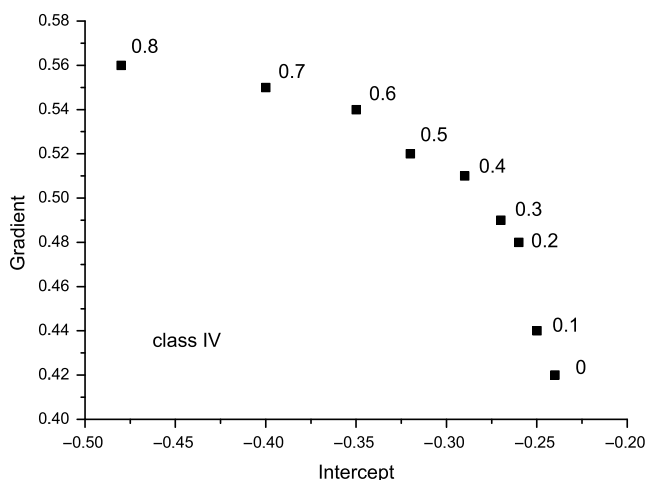


Figure 28. Intercept gradient plot corresponding to a source-rock layer of $h = 25$ m thickness and varying gas saturation S'_g . It corresponds to a transversely isotropic shale layer at a 3-km depth containing kerogen and gas embedded in a homogeneous isotropic shale without organic matter. The rock-physics model is Gassmann equation, and the frequency is 30 Hz.

high-velocity limestone. Also, the reflection coefficient (intercept) is increasing with maturity.

CONCLUSIONS

We propose a modeling methodology to build different RPT for source rocks containing organic matter, specifically, kerogen, oil, and gas. The fundamental aspects of shale oil and shale gas evolution from shales fully saturated with kerogen are considered by modeling the hydrocarbon generation and mineral diagenesis as a function of pressure, temperature, and burial depth. The rock-physics models are based on two dissimilar approaches, namely, Backus averaging and the Gassmann equation, which yield similar results in general, indicating the robustness of the methodology. RPTs are built, which are useful to evaluate kerogen content, hydrocarbon saturations, and in situ pore pressure. Mesoscopic-loss effects due to partial fluid saturations affecting wave velocities are

considered, but the Wood average is almost equivalent at seismic frequencies.

The creation of RPTs for a specific site requires calibration with well logs and information from related reports. This is performed for the Spekk Formation at the Norwegian Sea, where the Kimmeridge Shale is the main unit. Basically, the analysis is based on TOC values as a function of depth, which allows us to evaluate the kerogen content, as well as sonic and density logs to quantify the elastic properties of the minerals and shale frame. In the calibration process, at full kerogen saturation, Backus averaging and the Gassmann equation give practically the same results. Differences can be observed in the presence of hydrocarbon fluids, with Backus averaging predicting lower normal-bedding velocity at zero kerogen content, indicating that this model provides lower and upper limits. The main variations in the templates occur at low gas saturations and high oil saturations, with the Gassmann equation predicting lower V_p/V_s values, whereas the $\lambda - \mu - \rho$ templates are very similar. Wavefront representations indicate that the presence of fluids has decreased substantially the velocities and induce considerable S-wave splitting.

Pore pressure affects mainly the elasticity constants of the shale frame and in a lesser degree the bulk density through the gas density, whose changes with pore pressure are more remarkable than those of water and oil. We consider a specific sample of the Kimmeridge Shale to investigate the pressure effects. The bedding-normal P-wave velocity is highly affected by the pore pressure and the presence of fluids and the dry-rock velocities are generally higher due to the density effect. Unlike the case of varying gas saturation, the $\lambda - \mu - \rho$ template seems to discriminate the different pore pressures better than V_p/V_s versus AI, mainly when the pore pressure approaches the fracture pressure (or the confining pressure). Finally, we compute the reflection coefficient of a thin shale layer at a given depth saturated with kerogen and gas. The calculations, performed with two-term AVO, indicate that the behavior is class IV for any value of the gas saturation. Future work should consider two-term AVO including anisotropy.

ACKNOWLEDGMENTS

We thank Tullow Oil for funding the research and K. Bandyopadhyay, M. Yenugu, and an anonymous reviewer for useful comments.

APPENDIX A

OIL/GAS GENERATION AND SHALE DIAGENESIS

Let us assume a source rock at depth z . The lithostatic pressure for an average sediment density $\bar{\rho}$ is $p_c = \bar{\rho}gz$, where g is the acceleration of gravity. On the other hand, the hydrostatic pore pressure is approximately $p_H = \bar{\rho}_w gz$, where $\bar{\rho}_w$ is the density of water. For a constant sediment burial rate S and a constant geothermal gradient G , the temperature variation of a particular sediment volume is

$$T = T_0 + Gz = T_0 + Ht, \quad z = St, \quad H = GS, \quad (\text{A-1})$$

with a surface temperature T_0 at time $t = 0$, where t is the deposition time. Typical values of G range from 20 to 40°C/km, whereas S may range between 0.02 and 0.5 km/m.y. (m.y. = million years).

Kerogen/oil/gas conversion and overpressure

Assume that at time $t = 0$, corresponding to the surface, the shale contains kerogen at temperature T_0 and that the volume is "closed." The mass of convertible kerogen changes with deposition time t at a rate proportional to the mass present. Assuming a first-order kinetic reaction with the reaction rate given by the Arrhenius equation (Pepper and Corvi, 1995; Carcione, 2000; Pinna et al., 2011), the fraction of kerogen converted to oil (or fluid saturation s) satisfies the following equation:

$$\frac{\partial s}{\partial t} = -sA \exp[-E/RT(t)], \quad (\text{A-2})$$

where E is the activation energy, $R = 1.986 \text{ cal}/(\text{mol}^\circ\text{K})$ is the gas constant, A is the reaction rate at infinite temperature, and $T(t)$ is the absolute temperature. The solution is given below.

Let us obtain now the geopressure generated by the conversion of kerogen to oil in the presence of water (brine) in the pore space. We define the excess pore pressure by $\Delta p = p - p_i$, where p_i is the initial pore pressure and p is the pore pressure when a fraction s of kerogen mass has been converted to oil. Assume that the initial volumes of kerogen, water, and pore space are V_{ki} , V_{wi} , and V_{pi} , respectively. The definition of the respective bulk moduli is

$$\begin{aligned} K_o &= -V_o \frac{dp}{dV_o}, & K_k &= -V_k \frac{dp}{dV_k}, \\ K_w &= -V_w \frac{dp}{dV_w}, & K_p &= +V_p \frac{dp}{dV_p}, \end{aligned} \quad (\text{A-3})$$

where V_o is the oil volume equivalent to the amount of converted kerogen. The + sign means that the pore volume increases with increasing pore pressure because K_p is the bulk modulus at constant confining pressure. Integration of equations A-3 yields

$$\begin{aligned} V_o(p) &= V_{oi} \exp(-\Delta p/K_o), & V_k(p) &= V_{ki} \exp(-\Delta p/K_k), \\ V_w(p) &= V_{wi} \exp(-\Delta p/K_w), & V_p(p) &= V_{pi} \exp(+\Delta p/K_p). \end{aligned} \quad (\text{A-4})$$

Because the mass balance is independent of pressure, the amount of converted oil can be expressed as

$$\rho_o V_{oi} = s\rho_k V_{ki}, \quad (\text{A-5})$$

where ρ_o is the oil density, and V_{oi} and V_{ki} are the oil and kerogen volumes at p_i .

The pore volume at the initial pore pressure is $V_{pi} = V_{ki} + V_{wi}$ and the initial water saturation is $S_w = V_{wi}/V_{pi}$. Using A-5, the oil volume becomes

$$V_o(p) = sDV_{ki} \exp(-\Delta p/K_o), \quad (\text{A-6})$$

where $D = \rho_k/\rho_o$. Because at pressure p , the pore-space volume is

$$V_p = (1-s)V_k + V_o + V_w, \quad (\text{A-7})$$

we obtain

$$s = \frac{S_w \exp(-\Delta p/K_w) + (1 - S_w) \exp(-\Delta p/K_k) - \exp(\Delta p/K_p)}{(1 - S_w)[\exp(-\Delta p/K_k) - D \exp(-\Delta p/K_o)]}. \quad (\text{A-8})$$

This equation is equivalent to equation A-13 in Carcione (2000), which has a typographical error because the coefficient in the third exponential of the numerator is c_k instead of c_p .

The shale studied here is located at 3-km depth. The lithostatic pressure at this depth, for an average density of $\bar{\rho} = 2.4 \text{ g/cm}^{-3}$ is equal to $\bar{\rho}gz \simeq 70 \text{ MPa}$, where g is the acceleration of gravity. On the other hand, the hydrostatic pore pressure is approximately 30 MPa. Thus, the maximum possible pore-pressure change Δp will be from hydrostatic to lithostatic, i.e., almost 40 MPa (at this excess pressure, the rock may reach the fracturing stage). Because under these conditions, the arguments in the exponential functions in equation A-8 are much less than one, these functions can be approximated by $\exp(x) \simeq 1 + x$, $x \ll 1$, giving

$$\Delta p = \frac{s(1 - S_w)(D - 1)}{K_p^{-1} + K_k^{-1} + s(1 - S_w)(K_o^{-1}D - K_k^{-1}) - S_w(K_k^{-1} - K_w^{-1})}. \quad (\text{A-9})$$

Neglecting the mineral compressibility, the pore-space bulk modulus is given by $K_p = \phi K_m$, where K_m is the bulk modulus of the frame (see equation 7.76 in Carcione, 2015). Here, we consider that the pore-space bulk modulus depends linearly with the porosity as (Carcione, 2000)

$$K_p [\text{MPa}] = 2400 - 5400\phi', \quad (\text{A-10})$$

where $\phi' = \phi_k + \phi_w$ is the initial kerogen-plus-water proportion. Pore-space incompressibilities range from 240 to 2400 MPa, which correspond to compliant and rigid rocks, respectively.

Smectite/illite conversion

Pytte and Reynolds (1989) propose a model for the smectite/illite ratio r based on the n th-order Arrhenius-type reaction

$$\frac{\partial r}{\partial t} = -r^n A \exp(-E/RT(t)), \quad (\text{A-11})$$

where r is the smectite/illite ratio. The illite/smectite ratio in percent is 100 $(1 - r)$. The solution of equation A-11 is given in the next section.

Smectite is assumed isotropic and it is mixed with illite by Backus averaging (e.g., Carcione, 2015) to obtain the elasticity constants of the mineral composing the frame.

Solutions

Equations A-2 and A-11 are of the form

$$\frac{\partial y}{\partial t} = -y^n A \exp(-E/RT(t)), \quad (\text{A-12})$$

which has the solution

$$y(t) = m^{-1/m} \left\{ \frac{y_0^{-m}}{m} + \frac{A}{H} \left[\frac{E}{R} [\text{Ei}(x) - \text{Ei}(x_0)] + T \exp(x) - T_0 \exp(x_0) \right] \right\}^{-1/m}, \quad (\text{A-13})$$

where $m = n - 1$, $\text{Ei}(x)$ is the exponential integral,

$$x = -\frac{E}{RT}, \quad x_0 = -\frac{E}{RT_0}, \quad (\text{A-14})$$

where the dependence on the deposition time is given in the absolute temperature (see equation A-1).

The solution of equation A-2 ($n = 1$ and $s_0 = 1$) simplifies to

$$s = 1 - \exp \left\{ -\frac{A}{H} [TE_2(-x) - T_0E_2(-x_0)] \right\}, \quad (\text{A-15})$$

where

$$E_j(x) = \int_1^\infty \exp(-xq) \frac{dq}{q^j}. \quad (\text{A-16})$$

Equation A-13 can also be evaluated with E_1 using the relation $\text{Ei}(x) = -E_1(-x)$. Approximations to equation A-15 can be found in Berg and Gangi (1999), Carcione (2000), and Pinna et al. (2011).

APPENDIX B

EFFECTIVE FLUID MODEL FOR PARTIAL GAS SATURATION

The oil-gas mixture behaves as a composite fluid with properties depending on the constants of the constituents and their relative concentrations. The simplest solution to obtain its bulk modulus is to assume the Wood average:

$$K_f = \left(\frac{s_g}{K_g} + \frac{s_o}{K_o} \right)^{-1}, \quad (\text{B-1})$$

where $s_g = \phi_g/(\phi_g + \phi_o)$ denotes the gas saturation and $s_o = 1 - s_g$ is the oil saturation. Equation B-1 corresponds to the low-frequency limit. The density is

$$\rho_f = s_g \rho_g + s_o \rho_o. \quad (\text{B-2})$$

When the fluids are not mixed in the pore volume, but distributed in patches, the effective bulk modulus of the composite fluid is higher than that predicted by the Wood equation. We assume a simplified model, in which the frame is the kerogen and the fluids are oil and gas. White (1975) assumes spherical patches much larger than the grains, but much smaller than the wavelength. He develops the theory for a gas-filled sphere of porous medium of radius r_0 located inside a water-filled sphere of porous medium of outer radius r_1 ($r_0 < r_1$). The saturation of gas is

$$s_g = \frac{r_0^3}{r_1^3}, \quad s_o = 1 - s_g. \quad (\text{B-3})$$

The bulk modulus of the kerogen-oil-gas mixture is then given by the White (1975) expression, denoted by K_W (Carcione et al., 2006; Mavko et al., 2009). To obtain the effective fluid modulus K_f due to mesoscopic anelastic effects, we assume that K_W satisfies the Gassmann equation:

$$K_W = \frac{K_s - K_m + \varphi K_m (K_s/K_f - 1)}{1 - \varphi - K_m/K_s + \varphi K_s/K_f}, \quad (\text{B-4})$$

where $\varphi = \phi_f/(\phi_f + \phi_k)$, and we solve for K_f

$$K_f = \frac{\varphi K_s (K_W - K_m)}{K_s - (1 + \varphi) K_m - K_W (1 - \varphi - K_m/K_s)}. \quad (\text{B-5})$$

If φ exceeds a critical porosity value, say 0.5, K_f is the Wood modulus because the isostress condition holds.

APPENDIX C

DRY-ROCK ELASTICITY CONSTANTS AND PRESSURE EFFECTS

The Gassmann equation requires the knowledge of the dry-rock elasticity constants. Krief et al. (1990) propose a simple heuristic equation:

$$K_m = K_s (1 - \phi)^{A/(1-\phi)} \quad \text{and} \quad \mu_m = K_m \mu_s / K_s, \quad (\text{C-1})$$

where A is a constant, which depends on the type of rock (the second expression in equation C-1 is assumed here). The porosity dependence is consistent with the concept of critical porosity because the moduli should be small above a certain value of the porosity (usually between 0.4 and 0.6; Mavko and Mukerji, 1998).

The properties of the frame can be described by an anisotropic version of the Krief model:

$$\begin{aligned} c_{11}^m &= c_{11}^s g(A), \\ c_{66}^m &= c_{66}^s g(A), \\ c_{13}^m &= c_{13}^s g(B), \\ c_{33}^m &= c_{33}^s g(B), \\ c_{55}^m &= c_{55}^s g(B), \end{aligned} \quad (\text{C-2})$$

where

$$g(x) = (1 - \phi)^{x/(1-\phi)}, \quad (\text{C-3})$$

and A and B are constants. The use of two constants is somehow equivalent to vary the Krief exponent as a function of the propagation (phase) angle because c_{11}^m and c_{66}^m describe the velocities along the stratification, and c_{33}^m and c_{55}^m along the perpendicular direction. It is $A < B$, indicating that the critical porosity value is larger for the elastic constants describing the properties along the layering; i.e., the skeleton is mainly defined by these constants at high porosity (Carcione et al., 2011). Equation C-2 is reduced to equation C-1 for $A = B$ in the isotropic case. Another possibility is to obtain the dry-rock elasticity constants from wet-rock data by the inverse Gassmann relation (see Carcione et al., 2011).

A model completely based on data to model pore pressure effects can be obtained by the inverse Gassmann equation (Carcione et al., 2011). We use this equation to obtain the dry-rock stiffness constants from experimental data with 100% kerogen occupying the pore space and assuming an exponential dependence on the differential pressure p_d (Kaselow and Shapiro, 2004; Carcione et al., 2011).

APPENDIX D

LIST OF SYMBOLS

sub and superscripts	= $sm, i, m, w,$ and k : smectite, illite, matrix, water, and kerogen
sub and superscripts	= $o, g, s, f, if,$ and p : oil, gas, solid, fluid, pore-infill, and pore
E	= activation energy
A	= infinite-temperature rate
R	= gas constant
API	= oil API gravity
s_c	= weight fraction of sodium chloride
S	= sedimentation rate
G	= geothermal gradient
T	= temperature
t	= deposition time
z	= depth
g	= acceleration of gravity
s	= kerogen/oil or oil/gas fraction
r	= smectite/illite fraction
r_0	= initial smectite fraction or gas patch radius
p_c	= confining pressure
p_H	= hydrostatic pressure
p	= pore pressure
$p_d = p_c - p$	= differential (effective) pressure
Δp	= excess pore pressure
V	= volume
A, B	= Krief parameters
K	= bulk modulus
μ	= shear modulus
λ, μ	= Lamé constants
ρ	= shale density
Y	= Young modulus
ν	= Poisson ratio
ρ_s	= smectite-illite density
$\bar{\rho}_s$	= smectite-illite-water density
V_P, V_S	= P- and S-wave velocities
θ	= phase angle (propagation direction) or incidence plane-wave angle
V_p, V_e	= phase and energy velocities
c_{IJ}	= elasticity constants of the single constituents
\bar{c}_{IJ}	= elasticity constants of the shale
ϵ, δ, γ	= anisotropy parameters
V_{IJ}	= wave velocities
I_P, I_S	= P- and S-wave impedances
ϕ	= proportions
$\phi_{OC} = \phi_k + \phi_o + \phi_g$	= organic content
$\phi = \phi_w + \phi_o + \phi_g$	= porosity
$K = 100\phi_k$	= kerogen content (volume percent)

TOC = total organic content (weight per cent)
 S, S', s. = saturations

REFERENCES

- Avseth, P., T. Mukerji, and G. Mavko, 2005, Quantitative seismic interpretation: Cambridge University Press.
- Ba, J., J. M. Carcione, O. Du, H. Zhao, and T. M. Müller, 2015, Seismic exploration of hydrocarbons in heterogeneous reservoirs, new theories, methods and applications: Elsevier Science.
- Batzle, M., and Z. Wang, 1992, Seismic properties of pore fluids: *Geophysics*, **57**, 1396–1408, doi: [10.1190/1.1443207](https://doi.org/10.1190/1.1443207).
- Berg, R. R., and A. F. Gangi, 1999, Primary migration by oil-generation microfracturing in low-permeability source rocks: Application to the Austin Chalk, Texas: *AAPG Bulletin*, **83**, 727–756.
- Carcione, J. M., 2000, A model for seismic velocity and attenuation in petroleum source rocks: *Geophysics*, **65**, 1080–1092, doi: [10.1190/1.1444801](https://doi.org/10.1190/1.1444801).
- Carcione, J. M., 2001a, Amplitude variations with offset of pressure-seal reflections: *Geophysics*, **66**, 283–293, doi: [10.1190/1.1444907](https://doi.org/10.1190/1.1444907).
- Carcione, J. M., 2001b, AVO effects of a hydrocarbon source-rock layer: *Geophysics*, **66**, 419–427, doi: [10.1190/1.1444933](https://doi.org/10.1190/1.1444933).
- Carcione, J. M., 2015, Wave fields in real media: Theory and numerical simulation of wave propagation in anisotropic, anelastic, porous and electromagnetic media, 3rd ed.: Elsevier Science.
- Carcione, J. M., and F. Cavallini, 2002, Poisson's ratio at high pore pressure: *Geophysical Prospecting*, **50**, 97–106, doi: [10.1046/j.1365-2478.2002.00299.x](https://doi.org/10.1046/j.1365-2478.2002.00299.x).
- Carcione, J. M., H. Helle B., J. E. Santos, and C. L. Ravazzoli, 2005, A constitutive equations and generalized Gassmann modulus for multi-mineral porous media: *Geophysics*, **70**, no. 2, N17–N26, doi: [10.1190/1.1897035](https://doi.org/10.1190/1.1897035).
- Carcione, J. M., H. B. Helle, and P. Avseth, 2011, Source-rock seismic-velocity models: Gassmann versus Backus: *Geophysics*, **76**, no. 5, N37–N45, doi: [10.1190/geo2010-0258.1](https://doi.org/10.1190/geo2010-0258.1).
- Carcione, J. M., S. Picotti, D. Gei, and G. Rossi, 2006, Physics and seismic modeling for monitoring CO₂ storage: Pure and Applied Geophysics, **163**, 175–207, doi: [10.1007/s00024-005-0002-1](https://doi.org/10.1007/s00024-005-0002-1).
- Castagna, J. P., and H. W. Swan, 1997, Principles of AVO crossplotting: The Leading Edge, **16**, 337–344, doi: [10.1190/1.1437626](https://doi.org/10.1190/1.1437626).
- Cerón, M., J. D. Walls, and E. Diaz, 2013, Comparison of reservoir quality from La Luna, Gacheta and Eagle Ford Shale Formations using digital rock physics: Presented at AAPG Annual Convention and Exhibition.
- Chi, X.-G., and D.-H. Han, 2009, Lithology and fluid differentiation using rock physics templates: The Leading Edge, **28**, 60–65, doi: [10.1190/1.3064147](https://doi.org/10.1190/1.3064147).
- Ciz, R., and S. A. Shapiro, 2007, Generalization of Gassmann equations for porous media saturated with a solid material: *Geophysics*, **72**, no. 6, A75–A79, doi: [10.1190/1.2772400](https://doi.org/10.1190/1.2772400).
- Ebukanson, E. J., and R. R. F. Kinghorn, 1990, Jurassic mudrock formations of southern England: Lithology, sedimentation rates and organic carbon content: *Journal of Petroleum Geology*, **13**, 221–228, doi: [10.1111/j.1747-5457.1990.tb00841.x](https://doi.org/10.1111/j.1747-5457.1990.tb00841.x).
- Gei, D., and J. M. Carcione, 2003, Acoustic properties of sediments saturated with gas hydrate, free gas and water: *Geophysical Prospecting*, **51**, 141–158, doi: [10.1046/j.1365-2478.2003.00359.x](https://doi.org/10.1046/j.1365-2478.2003.00359.x).
- Helbig, K., 1994, Foundations of anisotropy for exploration seismics: Pergamon Press.
- Kaselow, A., and S. A. Shapiro, 2004, Stress sensitivity of elastic moduli and electrical resistivity in porous rocks: *Journal of Geophysics and Engineering*, **1**, 1–11, doi: [10.1088/1742-2132/1/1/001](https://doi.org/10.1088/1742-2132/1/1/001).
- Krief, M., J. Garat, J. Stellingwerff, and J. Ventre, 1990, A petrophysical interpretation using the velocities of P and S waves (full waveform sonic): *The Log Analyst*, **31**, 355–369.
- Kuster, G. T., and M. N. Toksöz, 1974, Velocity and attenuation of seismic waves in two-phase media. Part I: Theoretical formulations: *Geophysics*, **39**, 587–606, doi: [10.1190/1.1440450](https://doi.org/10.1190/1.1440450).
- Langrock, U., 2004, Late Jurassic to Early Cretaceous black shale formation and paleoenvironment in high northern latitudes: *Ber Polarforsch Meeresforsch*, **472**, 144.
- Mavko, G., and T. Mukerji, 1998, Comparison of the Krief and critical porosity models for prediction of porosity and V_p/V_s : *Geophysics*, **63**, 925–927, doi: [10.1190/1.1444403](https://doi.org/10.1190/1.1444403).
- Mavko, G., T. Mukerji, and J. Dvorkin, 2009, The rock physics handbook: Tools for seismic analysis in porous media: Cambridge University Press.
- Mondol, N. H., J. Jahren, K. Bjørlykke, and I. Brevik, 2008, Elastic properties of clay minerals: The Leading Edge, **27**, 758–770, doi: [10.1190/1.2944161](https://doi.org/10.1190/1.2944161).
- Ødegaard, E., and P. Avseth, 2004, Well log and seismic data analysis using rock physics templates: *First Break*, **23**, 37–43.
- Pepper, A. S., and P. J. Corvi, 1955, Simple kinetic models of petroleum formation. Part I: oil and gas generation from kerogen: *Marine and Petroleum Geology*, **12**, 291–319.
- Pinna, G., J. M. Carcione, and F. Poletto, 2011, Kerogen to oil conversion in source rocks: Pore-pressure build-up and effects on seismic velocities: *Journal of Applied Geophysics*, **74**, 229–235, doi: [10.1016/j.jappgeo.2011.05.006](https://doi.org/10.1016/j.jappgeo.2011.05.006).
- Pytte, A. M., and R. C. Reynolds, 1989, The thermal transformation of smectite to illite, in N. D. Naeser, and T. H. McCulloh, eds., Thermal history of sedimentary basins: Methods and case histories: Springer Verlag, 133–140.
- Sayers, C. M., 2013, The effect of anisotropy on the Young's moduli and Poisson's ratios of shales: *Geophysical Prospecting*, **61**, 416–426, doi: [10.1111/j.1365-2478.2012.01130.x](https://doi.org/10.1111/j.1365-2478.2012.01130.x).
- Schoenberg, M., and F. Muir, 1989, A calculus for finely layered media: *Geophysics*, **54**, 581–589, doi: [10.1190/1.1442685](https://doi.org/10.1190/1.1442685).
- Scotchman, I. C., 1987, Clay diagenesis in the Kimmeridge clay formation, onshore UK, and its relation to organic maturation: *Mineralogical Magazine*, **51**, 535–551, doi: [10.1180/minmag.1987.051.362.08](https://doi.org/10.1180/minmag.1987.051.362.08).
- Sondergeld, C. H., K. E. Newsham, J. T. Comisky, M. C. Rice, and C. S. Rai, 2010, Petrophysical considerations in evaluating and producing shale gas resources: Presented at SPE Unconventional Gas Conference, 131768-PP.
- Thomsen, L., 1986, Weak elastic anisotropy: *Geophysics*, **51**, 1954–1966, doi: [10.1190/1.1442051](https://doi.org/10.1190/1.1442051).
- Thyberg, B. I., J. Jahren, T. Winje, K. Bjørlykke, and J. I. Faleide, 2009, From mud to shale: Rock stiffening by micro-quartz cementation: *First Break*, **27**, 27–33, doi: [10.3997/1365-2397.2009003](https://doi.org/10.3997/1365-2397.2009003).
- Totten, M. W., M. A. Hanan, D. Knight, and J. Borges, 2002, Characteristics of mixed-layer smectite/illite density separates during burial diagenesis: *American Mineralogist*, **87**, 1571–1579.
- Vernik, L., 1994, Hydrocarbon-generation-induced microcracking of source rocks: *Geophysics*, **59**, 555–563, doi: [10.1190/1.1443616](https://doi.org/10.1190/1.1443616).
- Vernik, L., 1995, Petrophysics of the Kimmeridge shale, North Sea: Stanford Rock Physics Laboratory.
- Vernik, L., and C. Landis, 1996, Elastic anisotropy of source rocks: Implications for hydrocarbon generation and primary migration: *AAPG Bulletin*, **80**, 531–544.
- Vernik, L., and J. Milovac, 2011, Rock physics of organic shales: The Leading Edge, **30**, 318–323, doi: [10.1190/1.3567263](https://doi.org/10.1190/1.3567263).
- Vernik, L., and A. Nur, 1992, Ultrasonic velocity and anisotropy of hydrocarbon source rocks: *Geophysics*, **57**, 727–735, doi: [10.1190/1.1443286](https://doi.org/10.1190/1.1443286).
- Wang, Z. Z., H. Wang, and M. E. Cates, 2001, Effective elastic properties of solid clays: *Geophysics*, **66**, 428–440, doi: [10.1190/1.1444934](https://doi.org/10.1190/1.1444934).
- White, J. E., 1975, Computed seismic speeds and attenuation in rocks with partial gas saturation: *Geophysics*, **40**, 224–232, doi: [10.1190/1.1440520](https://doi.org/10.1190/1.1440520).
- Williams, C. J., S. P. Hesselbo, H. C. Jenkyns, and H. S. Morgans-Bell, 2001, Quartz silt in mudrocks as a key to sequence stratigraphy (Kimmeridge Clay Formation, Late Jurassic, Wessex Basin, UK): *Terra Nova*, **13**, 449–455, doi: [10.1046/j.1365-3121.2001.00378.x](https://doi.org/10.1046/j.1365-3121.2001.00378.x).
- Yenugu, M., and D.-H. Han, 2013, Seismic characterization of kerogen maturity: An example from Bakken shale: 83rd Annual International Meeting, SEG, Expanded Abstracts, 2773–2777.
- Zhu, Y., S. Xu, E. Liu, M. A. Payne, and M. J. Terrell, 2013, Predicting anisotropic source rock properties from well data: U.S. Patent 2013/0013209 A1.
- Zhu, Y., S. Xu, M. Payne, A. Martinez, E. Liu, C. Harris, and K. Bandyopadhyay, 2012, Improved rock-physics model for shale gas reservoirs: 82nd Annual International Meeting, SEG, Expanded Abstracts, doi: [10.1190/segam2012-0927.1](https://doi.org/10.1190/segam2012-0927.1).